MOLECULAR AND CELLULAR BIOLOGY, June 2006, p. 4185–4200 Vol. 26, No. 11
0270-7306/06/$08.00+0 doi:10.1128/MCB.01055-05

N-Cadherin and Keratinocyte Growth Factor Receptor Mediate the Functional Interplay between Ki-*RAS*^{G12V} and *p53*^{V143A} in Promoting Pancreatic Cell Migration, Invasion, and Tissue Architecture Disruption

Therese B. Deramaudt,[1,2] Munenori Takaoka,[1,2] Rabi Upadhyay,[5] Mark J. Bowser,[1,2] Jess Porter,[1,2] Amy Lee,[1,2] Ben Rhoades,[1,2] Cameron N. Johnstone,[1,2] Ralph Weissleder,[5] Sunil R. Hingorani,[2,4] Umar Mahmood,[5] and Anil K. Rustgi[1,2,3,4]*

Gastroenterology Division,[1] Department of Medicine,[2] Department of Genetics,[3] and Abramson Family Cancer Center and Family Cancer Research Institute,[4] University of Pennsylvania, Philadelphia, Pennsylvania, and Center for Molecular Imaging Research, Massachusetts General Hospital, Harvard Medical School, Boston, Massachusetts[5]

Received 7 June 2005/Returned for modification 10 July 2005/Accepted 17 March 2006

The genetic basis of pancreatic ductal adenocarcinoma, which constitutes the most common type of pancreatic malignancy, involves the sequential activation of oncogenes and inactivation of tumor suppressor genes. Among the pivotal genetic alterations are Ki-*RAS* oncogene activation and *p53* tumor suppressor gene inactivation. We explain that the combination of these genetic events facilitates pancreatic carcinogenesis as revealed in novel three-dimensional cell (spheroid cyst) culture and in vivo subcutaneous and orthotopic xenotransplantation models. N-cadherin, a member of the classic cadherins important in the regulation of cell-cell adhesion, is induced in the presence of Ki-*RAS* mutation but subsequently downregulated with the acquisition of *p53* mutation as revealed by gene microarrays and corroborated by reverse transcription-PCR and Western blotting. N-cadherin modulates the capacity of pancreatic ductal cells to migrate and invade, in part via complex formation with keratinocyte growth factor receptor and neural cell adhesion molecule and in part via interaction with p120-catenin. However, modulation of these complexes by Ki-RAS and p53 leads to enhanced cell migration and invasion. This preferentially induces the downstream effector AKT over mitogen-activated protein kinase to execute changes in cellular behavior. Thus, we are able to define molecules that in part are directly affected by Ki-RAS and p53 during pancreatic ductal carcinogenesis, and this provides a platform for potential new molecularly based therapeutic interventions.

There are nearly 30,000 new cases of pancreatic ductal adenocarcinoma each year. As such, there are about an equivalent number of pancreatic cancer-related deaths annually (11). Pancreatic ductal adenocarcinoma is the fourth leading cause of cancer-related deaths and carries with it a dismal prognosis with median survival of 6 months and 5-year survival of less than 5% (55). A subset of patients who have surgically resectable disease harbor 5-year survival rates of 15 to 20% (55). Overall, the poor prognosis is the result of anatomic considerations, nonspecific clinical manifestations, and presentation of patients at late stages when therapeutic modalities are palliative in nature. However, some progress is occurring with the development of adjuvant chemotherapy for locally advanced disease and with the potential employment of experimental therapeutic strategies involving immunotherapy.

While there is a complex interplay of genetic and environmental events that cooperate to facilitate initiation and promotion of pancreatic cancer, certain well-accepted genetic alterations are known to be of paramount importance. Point mutations in codon 12 of the Ki-*RAS* oncogene are the most frequent genetic alterations found in premalignant and advanced stages of pancreatic ductal adenocarcinoma (5, 46). Cooperating events with *HER2/NEU* overexpression, *CDKN2A*/*p16*^{INK4A} inactivation, *p53* mutations, *SMAD4* mutations, and *BRCA2* mutations are recognized to be necessary for progression from pancreatic preneoplastic lesions, termed PanIN for pancreatic intraepithelial neoplasia, to frank pancreatic cancer (27). The frequency of Ki-*RAS* oncogene mutations approaches 100% in early PanIN lesions and cancers that arise thereof (27). Inactivating mutations or deletions in the *CDKN2A*/*p16*^{INK4a} tumor suppressor gene increase in advanced PanIN lesions and occur in about 90 to 95% of ductal adenocarcinomas (14, 45). Missense point mutations in the *p53* tumor suppressor gene are most frequently observed in codons 143 and 175 (41) in 70% of pancreatic ductal adenocarcinomas. Mutation of the *SMAD4* tumor suppressor gene is noted in about 55% of pancreatic ductal adenocarcinomas and in about 30% of pancreatic intraepithelial neoplasia 3 lesions (56). Mutations in *BRCA2* and *STK1*/*LKB1* are found in up to 10% of pancreatic ductal adenocarcinomas. Genomic approaches are yielding promising clues about the involvement of other genes and gene loci (3). Yet how these genetic alterations contribute mechanistically to pancreatic carcinogenesis, either individually or in combination, remains to be elucidated.

Recently, several mouse models recapitulating the critical elements involved in the different stages of the human pancreatic cancers have been generated (2, 23, 26, 34, 53); these provide exciting opportunities for translation into potentially

* Corresponding author. Mailing address: University of Pennsylvania, 415 Curie Boulevard, Philadelphia, PA 19104-2144. Phone: (215) 898-0154. Fax: (215) 573-5412. E-mail: anil2@mail.med.upenn.edu.

novel methods for early detection and therapy. While Ki-*RAS* and *p53* mutations are critical, it is not known how they cooperate to promote pancreatic carcinogenesis and whether cell-specific and tissue-specific mechanisms might account for their aberrant biological and functional properties. This has led us to attempt to define and elucidate how Ki-*RAS* and *p53* cooperate in the context of pancreatic carcinogenesis. Recently, our laboratory has described a mouse model with Ki-RAS^{G12V} under the control of the cytokeratin 19 (K19) promoter. These *K19*-Ki-RAS^{G12V} transgenic mice develop hyperplastic lesions in pancreatic ducts with periductal lymphocytic infiltration but without ductal adenocarcinoma (13). We have isolated and characterized pancreatic ductal cells (PDC) from *K19*-Ki-RAS^{G12V} mice and their age-matched wild-type (WT) littermates (44). We find that the effects of oncogenic Ki-RAS^{G12V} are counterbalanced by upregulation of the cell cycle regulators $p16^{INK4a}$/$p19^{Arf}$ and $p27^{Kip1}$, allowing a controlled, regulatable cellular proliferation without induction of a senescent state. This may help explain why mutant Ki-*RAS* is necessary to initiate pancreatic ductal carcinogenesis but requires other genetic alterations to induce mature cancer (44), and it has prompted us to focus upon the *p53* tumor suppressor gene in cooperation with Ki-*RAS*.

The manner in which cells communicate with neighboring cells and the surrounding stroma entails intricate regulation. One of these regulators belongs to the cadherin family of molecules, which foster homotypic cell-cell adhesion. Two critical members of this family, involved in normal cell-cell contact, are E-cadherin and N-cadherin (50, 52). Loss of E-cadherin is associated with tumorigenesis (9, 40, 49, 51). Recent evidence suggests that N-cadherin may facilitate lateral dimerization of growth factor receptors, such as fibroblast growth factor receptors (FGFRs), and other molecules, such as neural cell adhesion molecule (N-CAM), and thereby stimulate signaling pathways leading to changes in cell behavior (38). Cavallaro et al. have recently reported that N-CAM may modulate the dissemination of metastatic tumor cells from pancreatic β-cells via the formation of a signaling complex involving FGFR-4 and N-cadherin, therefore activating several signal transduction pathways that lead to increased cell-matrix adhesion (16). Furthermore, the level or cellular localization of p120-catenin may be regulated by N-cadherin (35, 36, 57), which in turn may influence cell migration.

We explain herein that pancreatic ductal cells derived from *K19*-Ki-RAS^{G12V} transgenic mice, designated Ki-RAS^{G12V}-PDC, become tumorigenic when retrovirally transduced with $p53^{V143A}$. The tumorigenicity is found in soft agar assays and subcutaneous and orthotopic xenotransplantation mouse studies, in the latter of which tumors are monitored by in vivo bioluminescence. Ki-RAS^{G12V}/$p53^{V143A}$-PDC downregulate N-cadherin, resulting in increased cell migration and invasion, properties not present in PDC derived from wild-type, Ki-RAS^{G12V}, or $p53^{V143A}$ cells. The cellular events in the Ki-RAS^{G12V}/$p53^{V143A}$-PDC can be recapitulated by biochemical and genetic disruption of N-cadherin or keratinocyte growth factor receptor (KGFR). In addition, the level of p120-catenin, which interacts with N-cadherin, is influenced by the level of N-cadherin expression, and may modulate the extent of adherens junction formation and provide a basis for cell migration, in part through phosphorylation of AKT. These molecules are for the first time shown to be involved in the regulation of migration and invasion of pancreatic ductal epithelial cells and serve as a basis for understanding a molecular mechanism for the cooperation of Ki-RAS^{G12V} and $p53^{V143A}$.

MATERIALS AND METHODS

Substrates and antibodies. Matrigel and rat tail type I collagen were obtained from BD Biosciences (Bedford, MA). All transfections were performed using Lipofectamine 2000 (Invitrogen, Carlsbad, CA) by following the manufacturer's instructions. Restriction endonuclease enzymes EcoRI, AvaI, and HincII were purchased from New England BioLabs (Beverley, MA). The AKT-specific inhibitor AKTi1/2, the phosphatidylinositol 3-kinase (PI3K) inhibitor LY294002, and the MEK inhibitor U0126 were obtained from Calbiochem (San Diego, CA).

Mouse monoclonal neutralizing antibody against the cytoplasmic tail of N-cadherin (A-CAM clone GC-4) and anti-β-actin were obtained from Sigma (Dallas, TX). Mouse monoclonal anti-N-cadherin, anti-E-cadherin, anti-β-catenin, anti-p120-catenin, anti-beta-1 integrin, and anti-pan N-CAM antibodies were obtained from BD Transduction (San Diego, CA). Rabbit polyclonal anti-FGFR-1, -2, -3, and -4 were purchased from Santa Cruz Biotechnology Inc. (Santa Cruz, CA). Rabbit polyclonal anti-phospho-AKT (Ser473), anti-AKT, anti-phospho-p44/42 mitogen-activated protein kinase (MAPK) (Thr202/Tyr204), and anti-p44/42 MAPK were purchased from Cell Signaling Technology (Beverly, MA). Horseradish peroxidase-conjugated sheep anti-mouse or donkey anti-rabbit immunoglobulin G (IgG) was obtained from Amersham (Piscataway, NJ). Cy3-conjugated goat anti-mouse antibody was obtained from Jackson ImmunoResearch Laboratories (West Grove, PA).

Cell culture. Primary PDC, Ki-RAS^{G12V}-PDC, and WT-PDC were established from transgenic *K19*-Ki-RAS^{G12V} mice and their age-matched wild-type littermates as previously described (44). The cells were routinely maintained at 37°C in a 5% CO_2 humidified incubator in Dulbecco's modified Eagle's medium (DMEM)/F12 full medium containing 5 mg/ml D-glucose, 0.1 mg/ml soybean trypsin inhibitor type I, 5 nM 3,3′,5-triiodo-L-thyronine, 1 μM dexamethasone, 10 mM nicotinamide, and 100 ng/ml cholera toxin, all purchased from Sigma; and 5 ml/liter insulin-transferrin-selenium, 25 μg/ml bovine pituitary extract, 20 ng/ml epidermal growth factor, and 5% Nu-serum IV culture supplement from BD Biosciences.

For three-dimensional cultures, pancreatic ductal cells were grown to confluence as a monolayer and then trypsinized. Single cells (1×10^4 cells) were suspended in a mix of 0.4 mg/ml rat tail collagen type I in DMEM/F12 full medium as described above and plated in four-chamber slides precoated with 100 μl/chamber of 2.3-mg/ml rat tail collagen type I. For three-dimensional cultures in Matrigel, cells were embedded in 2% Matrigel mixed with DMEM/F12 full medium and laid on a culture dish precoated with 100% Matrigel. Cultures were then grown for 7 to 14 days in these chamber slides, and the medium was replaced every 4 days.

Retroviral vectors and transduction. The cDNA of mouse N-cadherin was amplified by reverse transcription-PCR (RT-PCR) using total RNA isolated from WT-PDC and specific primers, including EcoRI sites (sense, 5′-AGAAG AATTCTCTCCGCCTCCATGTGCCGG-3′; antisense, 5′-AGAAGAATTCTC AGTCGTCACCACCGCCGTAC-3′), and subcloned into the pBABE-hygromycin (hygro) retroviral vector (37). The inserted region was verified by DNA sequencing. By following the manufacturer's directions, the QuikChange (Stratagene, La Jolla, CA) site-directed mutagenesis method was used to generate the dominant negative mutant N-cadherin deleted at its extracellular domain (NcadΔECD).

The retroviral vector pFB-neo/*dnKGFR* expressing mouse dominant negative KGFR (FGFR-2; deletion of the cytoplasmic tail) was generated by digesting pMMTV/*fgfr-2(IIIb)*, kindly provided by C. Dickson (31), with the restriction enzyme EcoRI and by inserting the *fgfr-2(IIIb)* digested fragment into the EcoRI-linearized pFB-neomycin (neo) vector (Stratagene). The insert orientation was verified by PCR using the specific primers 5′pFB (sense, 5′-GGCTGC CGACCCCGGGGGTGG-3′) and FGF-RB (antisense, 5′-CCCGGGGAATTC ACCACCATGCAGGCGATTAA-3′). The pFB-neo/*luc* retroviral vector was generated by inserting a firefly luciferase reporter gene in pFB-neo (gift from W. El-Deiry).

pBABE-puro/$p53^{V143A}$, BABE-hygro/*NcadΔECD*, pFB-neo/*luc*, pFB-neo/*dnKGFR*, and the corresponding control vectors were transfected into the Phoenix ecotropic packaging cell line (gift from G. Nolan) using Lipofectamine 2000. Viral stock-containing supernatants were collected 48 and 72 h after transfection, filtered through a 0.45-μm-pore-size filter, and stored at −80°C until use.

In six-well plates, 70% confluent monolayers of primary pancreatic ductal cells

were infected with 0.4 ml of retroviral supernatants in the presence of Polybrene (Sigma). Each plate was centrifuged at room temperature for 45 min, and then the medium was replaced with fresh DMEM/F12 full medium. After 48 h, transduced cells were selected with 5 μg/ml of puromycin for 5 days, 150 μg/ml of hygromycin for 14 days, or 400 μg/ml of G418 for 4 days.

Microarray analysis. Total RNA was extracted from early population doublings of pancreatic ductal cell lines. For two-dimensional cultures, four replicates of WT-PDC and $p53^{V143A}$-PDC and two replicates of Ki-RAS^{G12V}-PDC and Ki-RAS^{G12V}/$p53^{V143A}$-PDC were submitted for microarray analysis through the Penn Microarray Facility. For three-dimensional cultures, duplicates of the four cell lines grown for 3 weeks in Matrigel matrix (BD Biosciences) were submitted for microarray analysis. Preparation of the cRNA and the subsequent microarray processes were performed as described in the Affymetrix GeneChip expression analysis technical manual (Affymetrix, Santa Clara, CA). Briefly, the culture medium was removed from the 10-cm plastic dishes, and exponentially growing cells were then immediately frozen in liquid nitrogen. Total RNA was extracted from the cells using TRIzol reagent (Invitrogen) and purified using RNeasy columns according to the manufacturer's protocol (QIAGEN, Valencia, CA). Total RNA (8 μg) was amplified and biotinylated by in vitro transcription. Fifteen micrograms of cRNA was hybridized to the Affymetrix MOE430 2.0 Mouse GeneChip. This array assays over 39,000 transcripts identified from public databases and mapped to genomic sequences. The Affymetrix GCS3000 laser scanner was used to scan fluorescent signals at 3-μm resolution after excitation at 570 nm. The average signal from two sequential scans was calculated for each microarray feature.

Primary analysis of high-throughout array data was performed using Affymetrix microarray suite 5.0 (Affymetrix) and Genespring 5.0 (Silicon Genetics, Redwood City, CA) software. GeneSpring was used to perform principal components analysis and to generate Venn diagrams. Genes that were flagged as being absent in all samples were removed from further analysis, and significant differential expression was defined as twofold change versus the respective controls.

RT-PCR analysis. Total RNA was isolated from monolayer cultures using Trizol reagent, and cDNA was synthesized by random priming from 1 μg of total RNA using a Superscript first-strand synthesis system (Invitrogen) according to the manufacturer's directions. The semiquantitative analysis of transcripts encoding N-cadherin and GAPDH was carried out with a mixture of cDNA derived from WT-PDC, Ki-RAS^{G12V}-PDC, $p53^{V143A}$-PDC, and Ki-RAS^{G12V}/$p53^{V143A}$-PDC; 0.2 μM each of the sense and antisense primers; 0.2 μM of deoxynucleoside triphosphate; and 2.5 U of *Pfu* Turbo DNA polymerase (Stratagene) in a final reaction volume of 50 μl. Mouse N-cadherin PCR primers (sense, 5′-GGCGTCTGTGGAGGCTTCTGGTGAA-3′; antisense, 5′-GTGATGACGGCTGTGGCTGTGTTTGA-3′) were used, generating a 1.1-kb cDNA fragment. The sequences of the primers for GAPDH, yielding a 440-bp cDNA product, were 5′-TGTGAACGGATTTGGCCGTA-3′ (sense) and 5′-AAGCAGTTGGTGGTGCAGGA-3′ (antisense). The PCR program was as follows: 90°C for 2 min; 30 cycles of 94°C for 30 s, 60°C for 30 s, and 68°C for 1 min; and a final extension at 68°C for 7 min. The data shown were obtained with 30 PCR cycles. Amplification of the exons upstream and downstream of the alternative exons IIIb and IIIc was described previously (15) and was achieved using the specific primers FGF-FB (5′-CCCGGGTCTAGATTTATAGTGATGCCCAGCCC-3′) and FGF-RB (see above). The PCR products were subjected to restriction endonuclease digestion with AvaI or HincII. Analysis of digested and undigested PCR products was done by electrophoresis on a 2% agarose gel.

Indirect immunofluorescence. For indirect immunofluorescence staining, cells grown on Lab-Tek four-chamber slides (Nunc, Naperville, IL) as monolayer or three-dimensional cultures were washed twice with phosphate-buffered saline (PBS) (pH 7.4), fixed in a 1:1 ratio of ice-cold methanol-acetone for 10 min, washed briefly with PBS, and then permeabilized with 0.1% Triton X-100 for 5 min. Cells were incubated with 1% bovine serum albumin (BSA)–PBS for 1 h at room temperature and then with the primary antibody diluted in 1% BSA–PBS for 1 h. After washing with PBS, the cells were incubated in the presence of Cy3-conjugated secondary antibodies for 1 h. For phalloidine staining, fixed cells were incubated with 0.1 μg/ml FITC-phalloidine (Sigma) for 1 h at room temperature. After washing twice with PBS and then with water, cells were counterstained with DAPI (4′,6′-diamidino-2-phenylindole). The slides were protected with cover slips using Vectashield (Vector Laboratories Inc., Burlingame, CA) and examined using a fluorescence microscope (E600 Nikon) and IPLab software for picture analysis or a confocal inverted fluorescence microscope (Zeiss Axiovert 200 M) and Zeiss LSM510META 3.2 software for picture analysis.

Immunoblotting and immunoprecipitation. For immunoblot analysis, cells were washed with PBS and lysed with RIPA buffer (150 mM NaCl, 1% Triton X-100, 0.5% sodium deoxycholate, 0.1% sodium dodecyl sulfate, 50 mM Tris-HCl [pH 7.5], and a cocktail of protease inhibitors [Complete mini; Roche, Indianapolis, IN]). Protein concentration was determined by the Bradford method (Bio-Rad, Hercules, CA). A total of 10 μg of total protein was resolved by sodium dodecyl sulfate–4 to 12% polyacrylamide gel electrophoresis and transferred to polyvinylidene difluoride membrane (Immobilon, Millipore Corp., Bedford, MA). Blocking was performed in 5% milk–1× TBST (10 mM Tris-HCl, pH 7.4, 150 mM NaCl, and 0.1% Tween 20) for 1 h before incubation with primary antibodies. Horseradish peroxidase-conjugated secondary antibodies were used according to the manufacturer's protocols. Immunoreactivity was visualized using the ECL+ system (Amersham) and was exposed to BioMax MR film (Eastman Kodak Co.). Immunoprecipitation was based upon previously described methods (8).

Migration and invasion assays. Migration assays were performed using Boyden chambers (8-μm-pore-size membranes), and invasion assays were performed using Boyden chambers coated with 125 μg/cm^2 of Matrigel (BD Biosciences). Inserts were placed in a 24-well plate containing DMEM/F12 full medium, which stimulates cell migration or invasion. Pancreatic ductal cells (5×10^4 cells/chamber) were resuspended in DMEM/F12 empty medium and added to each insert. After 24 h, the cells that did not migrate or invade were removed from the upper faces of the inserts using cotton swabs, and the cells that migrated to or invaded the lower surfaces of the inserts were fixed in methanol and stained using a Diff-Quick kit (Dade Behring Inc., Newark, DE). Each assay was performed in duplicate and repeated independently two to four times. The membranes were cut out and mounted on a glass slide, and migrating or invading cells were observed under the microscope (40× magnification). Ten pictures of individual fields were taken per membrane, and the numbers of cells were quantified. For specific conditions, cells were preincubated for 30 min in the presence of the N-cadherin neutralizing antibody GC-4 prior to plating in the Boyden chambers. LY294002, AKTi1/2, or U0126 was added in both the top and bottom chambers.

Soft agar assays. Control primary epithelial cell lines and those infected with the dominant negative $p53^{V143A}$ retrovirus were harvested for agar cloning. In six-well plates, 2×10^5 cells/well, suspended in 3 ml of 0.5% low melting agarose-DMEM-F12 full medium, were overlaid onto a base layer of 1% agarose-DMEM-F12 full medium. The cells were incubated for 3 weeks at 37°C in a humidified atmosphere containing 5% CO_2. Colony formation was assessed, and pictures were taken at 20× and 100× magnifications by using a phase-contrast microscope.

Subcutaneous and orthotopic (pancreatic) implantations in nude mice. Studies were carried out in accordance with protocols approved by the institutional Animal Care and Use Committee. WT/*luc*-PDC, Ki-RAS^{G12V}/*luc*-PDC, $p53^{V143A}$/*luc*-PDC, and Ki-RAS^{G12V}/$p53^{V143A}$-*luc*-PDC were obtained by stably transducing the cell lines with the retroviral vector pFB-neo/*luc*. For subcutaneous injections, 20 5- to 8-week-old female athymic mice (NCRNU-M; Taconic, Hudson, NY), divided into four groups of five mice and irradiated with 1.33 Gy/min, were subcutaneously injected in the dorsal flanks (three injection sites per mouse) with a 1:1 mix of Matrigel–DMEM-F12 full medium containing 1×10^7 of luciferase-expressing pancreatic ductal cells in suspension. Tumor volume measurements (length by width by depth) began 5 weeks after injection and were completed after 8 weeks of injections, and at 10 weeks the mice were sacrificed and any tumors were assessed by histology and immunohistochemistry. In addition, a separate cohort of four athymic mice that were not irradiated were injected independently with Ki-RAS^{G12V}/$p53^{V143A}$-*luc*-PDC in the same protocol, monitored for tumor growth, and sacrificed at 4, 6, and 10 weeks for evaluation by histology and immunohistochemistry.

For pancreatic orthotopic evaluation, the same four cell lines were implanted into 24 athymic mice (5 to 8 weeks old), divided into four groups of six mice. A small left-flank incision was made to expose the pancreas. Under direct visualization with the aid of a dissecting microscope, 2×10^6 cells mixed with a 1:1 ratio of Matrigel were injected deep into the pancreatic tail, and the incision was closed in two layers. There was no mortality associated with the procedure. Five weeks after implantation, bioluminescence and magnetic resonance (MR) imaging was performed.

In vivo bioluminescence imaging studies. D-Luciferin (50 mg/ml; Xenogen, Alameda, CA) was dissolved in sterile PBS and stored at −20°C. A 1:1 mix of D-luciferin (150 mg/kg of body weight) and anesthesia (ketamine; Sigma) was administered by intraperitoneal injection. Fifteen to twenty minutes after injection of the D-luciferin substrate, in vivo bioluminescent images were acquired noninvasively using the IVIS imaging system (Xenogen). Mice were placed in a light-tight chamber, with a field view set at 15 cm above the imaging stage, and dorsal images were collected for 1 min. Tumor growth was monitored weekly for 10 weeks. Grayscale reflected images and colorized bioluminescent images were

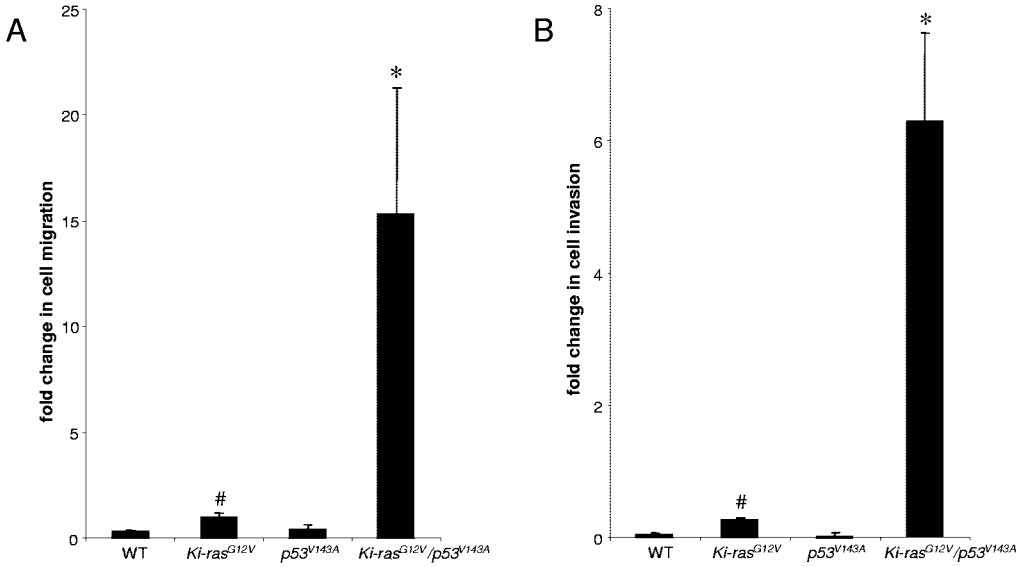

FIG. 1. Ki-*RAS*^{G12V}/*p53*^{V143A}-PDC display increased migration and invasion. (A) Pancreatic ductal cells representing the different genotypes were seeded on noncoated Boyden chamber membranes for migration assays. After 24 h, the cells that did not migrate were removed using cotton swabs. The migrating cells were stained and quantified by averaging 10 individual fields. (B) Pancreatic ductal cells representing the different genotypes were seeded on Matrigel-coated Boyden chamber membranes for invasion assays. After 24 h, the cells that did not invade were removed while the invading cells were stained and quantified by averaging 10 individual fields. Symbols: *, $P < 0.02$ (Ki-*RAS*^{G12V}/*p53*^{V143A}-PDC versus Ki-*RAS*^{G12V}-PDC or *p53*^{V143A}-PDC), #, $P < 0.05$ (Ki-*RAS*^{G12V}-PDC versus WT-PDC). The data were obtained from three independent experiments performed in duplicate.

superimposed. Photons emitted from the injected areas were quantified in photons per second using LivingImage software (Xenogen).

Bioluminescence imaging of pancreatic orthotopic tumors was similar to that described above, except that the animals were imaged using a left anterior oblique view to optimize imaging of the pancreatic tail. Image integration time was 5 min with 4 × 4 binning used to increase the signal from the deeper (orthotopic) tumors. MR imaging was performed with a small-animal Bruker 4.7T Pharmascan magnet, using a 38-mm-diameter mouse body transmit-receive radiofrequency coil (Bruker Biospin, Ettlingen, Germany). Animals were anesthetized with 1% isofluorane, and their respiratory rates were monitored. Coronal T1 weighted images taken after intraperitoneal gadolinium diethylene triamine pentaacetic acid (0.3 mmol/kg) (Magnevist; Schering, Berlin, Germany) administration were acquired without respiratory trigger through the upper abdomen. The following parameters were used for acquisition: rapid acquisition with relaxation enhancement sequence; field of view, 5.5 cm by 5.5 cm; matrix size, 256 by 256; slice thickness, 1 mm; echo time (effective), 15.3 ms; reaction time, 611 ms; number of averages = 12. These parameters resulted in a total acquisition time of 7 min 49 s and a voxel size of 1.0 by 0.2 by 0.2 mm.

Isolation of tumor cells and reinjection into recipient athymic nude mice. Briefly, 3 weeks after subcutaneous injections with Ki-*RAS*^{G12V}/*p53*^{V143A}-PDC (four dorsal-flank injection sites per mouse), one athymic nude mouse was sacrificed, and the subcutaneous tumors were collected and transferred into an STD solution (Leibovitz 15 solution containing 200 μg/ml methylcellulose, 15 μg/ml reduced glutathione, 4.3 ng/ml sodium selenite, 0.5% human serum albumin, 1.25 μg/ml fungizone, 100 U/ml penicillin, and 100 μg/ml streptomycin). The tumors were sliced with crossed scalpels, reduced into small segments of ~1 mm^3, and washed twice with PBS, and then tumor segments were plated on culture dishes precoated with collagen type I (44). Afterward, the tumor cells were cultured on plastic dishes. After G418 treatment to select for luciferase-expressing tumor cells, the cells were subcutaneously reinjected (1×10^7 cells per injection site) into two recipient athymic nude mice (NCRNU-M; Taconic) using the same conditions as described above. Bioluminescence imaging was performed weekly for 4 weeks by imaging mice injected in parallel with Ki-*RAS*^{G12V}/*p53*^{V143A}-PDC and tumor-derived Ki-*RAS*^{G12V}/*p53*^{V143A} cells.

Histology and immunohistochemistry. Paraffin-embedded murine tissues were processed by standard procedures. Briefly, excised tissues were fixed in 4% paraformaldehyde at 4°C for 24 h and then embedded in paraffin wax before sectioning. Tissue sections measuring 5 μm were deparaffinized, immersed in 10 mM citric acid buffer (pH 6.0), and microwaved for 6 min. Slides were washed, and the endogenous peroxidases were quenched by incubating the slides in 2.5% hydrogen peroxide for 15 min followed by successive blocking with Avidin D reagent, Biotin reagent (Vector Laboratories Inc.), and protein-blocking reagent (Coulter-Immunotech) for 15 min each. Slides were incubated at room temperature for 1 h with specific primary antibodies diluted in PBT (0.1% BSA and 0.2% Triton X-100 in PBS). After two washes with PBS, the slides were incubated for 1 h at room temperature with the biotinylated secondary antibodies. Peroxidase staining (DAB substrate kit for peroxidase) was performed as recommended by the manufacturer (Vector Laboratories, Inc). The primary antibodies employed were against vimentin (Novus Biologicals, Littleton, CO), S-100 (Nova Castra, Newcastle upon Tyne, United Kindom), E-cadherin (BD Transduction), and pancytokeratin (Sigma).

Densitometry measurements and statistical analysis. Densitometry measurements were performed using Scion Image Beta 4.02 software (Frederick, MD) and calibrated with GAPDH or β-actin signal. Analysis of variance (ANOVA) with a Tukey's post hoc test was used for statistical analysis. A P value of <0.05 was considered statistically significant.

RESULTS

Increased migration and invasiveness of Ki-*RAS*^{G12V}/*p53*^{V143A}-PDC. We derived pancreatic ductal cells from wild-type and *K19*-Ki-*RAS*^{G12V} mice by previously described methods and infected the primary cell lines with a retrovirus expressing the dominant negative *p53*^{V143A} (44). The ability of *p53*^{V143A} to suppress wild-type p53-mediated functions related to DNA damage response was confirmed (48; data not shown). To determine whether Ki-*RAS*^{G12V}/*p53*^{V143A}-PDC migrated and invaded to a greater extent than the parental cells, we performed well-established migration and invasion assays. After 24 h of incubation, Ki-*RAS*^{G12V}/*p53*^{V143A}-PDC demonstrated migration and invasiveness that were statistically significantly increased compared to WT-PDC, *p53*^{V143A}-PDC, and Ki-*RAS*^{G12V}-PDC (Fig. 1).

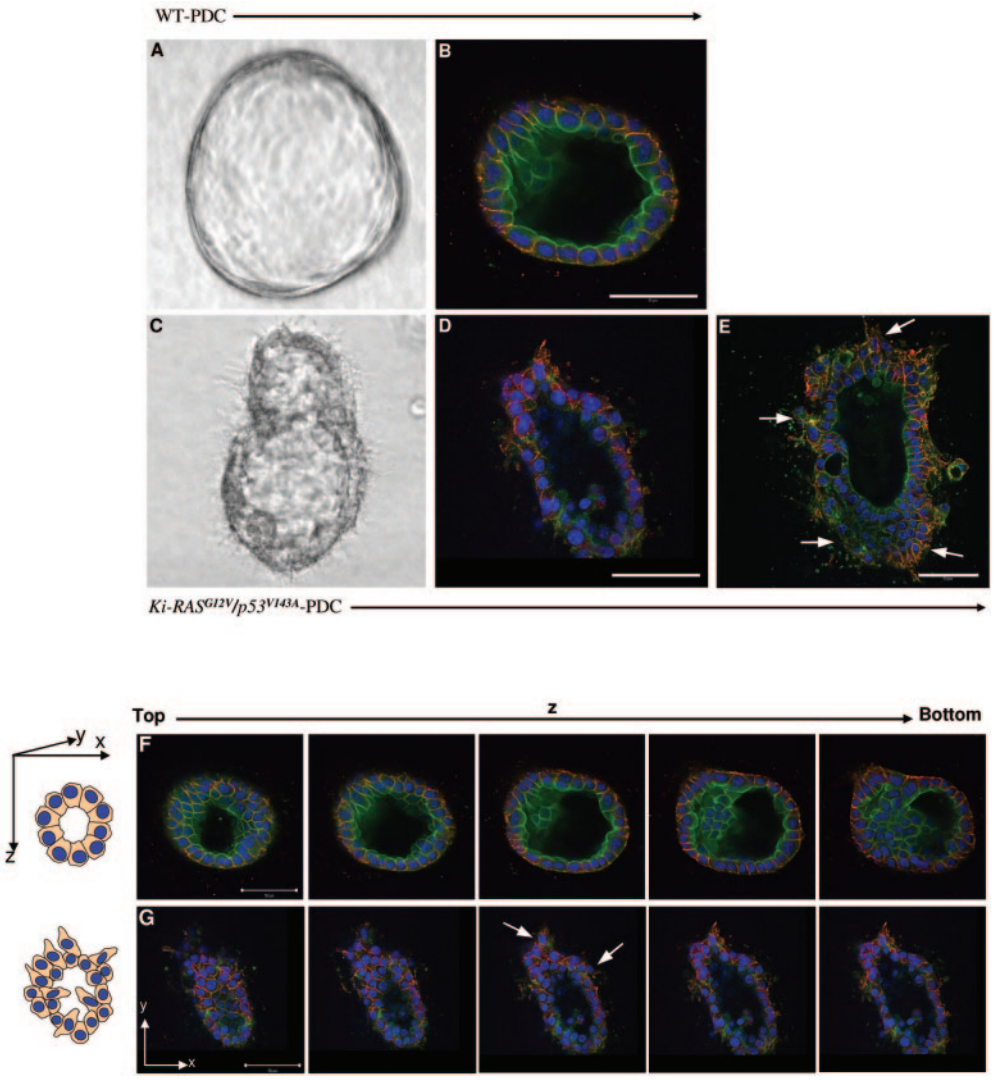

FIG. 2. Three-dimensional spheroid cysts derived from Ki-RAS^{G12V}/$p53^{V143A}$-PDC reveal disrupted cellular architecture. (A and B) Typical spheroid cyst from WT-PDC grown in collagen type I gel for 7 days. (A) Phase-contrast photomicrograph taken at ×100 magnification. (B) Confocal imaging of immunofluorescence staining of a methanol-acetone-fixed cyst stained for E-cadherin (red), actin (green), and DAPI (blue). (C to E) Disrupted spheroid cyst from Ki-RAS^{G12V}/$p53^{V143A}$-PDC grown in collagen type I matrix for 7 days. (C) Phase-contrast photomicrograph taken at ×100 magnification. (D to E) Confocal imaging of immunofluorescence staining of a methanol-acetone-fixed cyst of Ki-RAS^{G12V}/$p53^{V143A}$-PDC stained for E-cadherin (red), actin (green), and DAPI (blue). (F and G) Serial confocal microscopic cross sections of spheroid cysts derived from the PDC. (F) WT-PDC were cultured on type I collagen matrix for 7 days, immunostained for E-cadherin (red) as a basolateral marker and actin (green) as an apical marker, and DAPI counterstained for nuclei (blue). (G) Disrupted cellular architecture and loss of polarity were uniquely evident from Ki-RAS^{G12V}/$p53^{V143A}$-PDC derived spheroid cysts. Arrows indicate protruding cells. The top of the cyst appears as a sheet of cells. By contrast, the equatorial section appears as a ring due to the presence of a hollow lumen. Scale bars for all panels = 50 μm.

Ki-RAS^{G12V}/$p53^{V143A}$-PDC form cysts in three-dimensional culture that are disrupted compared to normal cysts derived from WT-PDC, $p53^{V143A}$-PDC, and Ki-RAS^{G12V}-PDC. Embedding pancreatic ductal cells in a type I collagen matrix leads to the formation of three-dimensional spheroid cysts (21, 44). A representative cyst formed from WT-PDC is composed of cuboidal monolayer cells enclosing a lumen (Fig. 2A). Identical spheroid cysts are also observed when culturing $p53^{V143A}$-PDC and Ki-RAS^{G12V}-PDC in a three-dimensional matrix (data not shown). The presence of a lumen precludes the notion that these cells are acinus-like. To determine whether these structures consist of cells that are organized and polarized, namely whether they form apical and basolateral surfaces as is the case with pancreatic ductal epithelial cells, the cysts were stained for specific markers by immunofluorescence. Indirect immunofluorescence staining with confocal microscopy for E-cadherin, a basolateral marker, and for actin, an apical marker, confirmed that the pancreatic ductal cells forming the cyst structures are polarized (Fig. 2B and F). After 1 week, the cells developed into organized cysts reminiscent of those formed from MCF-10A cells grown on reconstituted matrix gel or MDCK cells grown in collagen type I gel (17, 54).

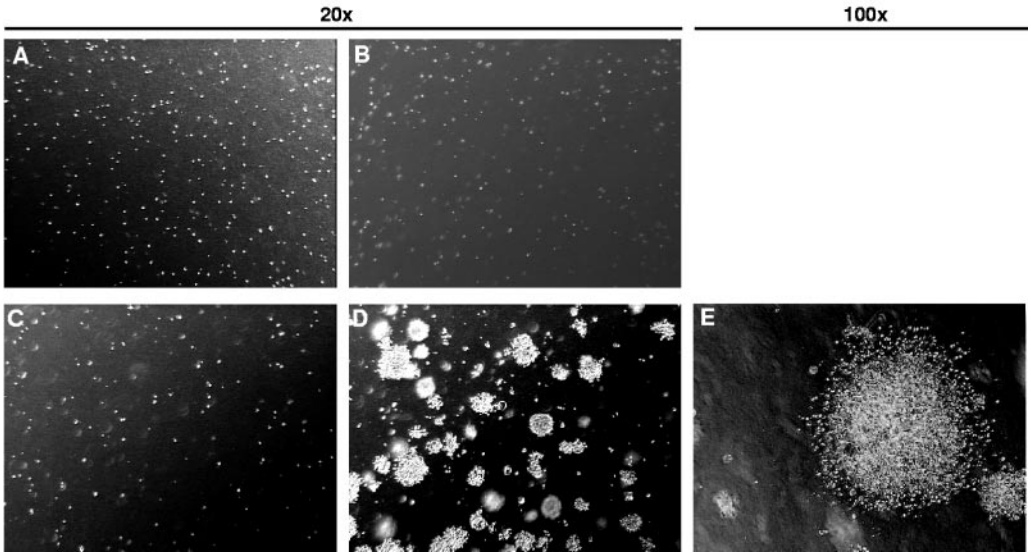

FIG. 3. Ki-RAS^{G12V}/$p53^{V143A}$-PDC grow in an anchorage-independent manner. In six-well culture plates, 2×10^5 cells suspended in 0.5% agarose/DMEM/F12 full medium were overlaid onto a base layer of 1% agarose–DMEM-F12 full medium. The cells were incubated for 3 weeks, and colonies were visualized by phase-contrast microscopy and photodocumented. Panels: (A) WT-PDC (magnification, ×20); (B) $p53^{V143A}$-PDC (magnification, ×20); (C) Ki-RAS^{G12V}-PDC (magnification, ×20); (D and E) Ki-RAS^{G12V}/$p53^{V143A}$-PDC (magnification, ×20 and ×100, respectively).

Although very few differences in morphology could be observed between WT-PDC, $p53^{V143A}$-PDC, Ki-RAS^{G12V}-PDC, and Ki-RAS^{G12V}/$p53^{V143A}$-PDC when cultured in monolayer, profound differences between these cells were observed when they were cultured in a three-dimensional matrix. Within 1 week, Ki-RAS^{G12V}/$p53^{V143A}$-PDC formed abnormal spheroid cysts with disruption of cellular architecture manifest by protrusion of cells along the surface and invasion of cells into the lumen, consistent with a potentially malignant phenotype (Fig. 2C to E and G) that was not observed in spheroid cysts derived from WT-PDC, $p53^{V143A}$-PDC, or Ki-RAS^{G12V}-PDC. As a parallel consideration, cells invading into the lumen were not found to undergo apoptosis (data not shown). In addition, immunofluorescence staining for E-cadherin and actin revealed a loss of cell polarity.

Expression of mutant $p53^{V143A}$ in Ki-RAS^{G12V}-PDC promotes cell tumorigenicity. Next, we wanted to determine the tumorigenicity of the various pancreatic ductal cell lines. For an initial assessment, soft agar assays were employed. WT-PDC, Ki-RAS^{G12V}-PDC, $p53^{V143A}$-PDC, and Ki-RAS^{G12V}/$p53^{V143A}$-PDC were plated on soft agar and permitted to grow for up to 3 weeks. While WT-PDC, Ki-RAS^{G12V}-PDC, and $p53^{V143A}$-PDC did not form colonies (Fig. 3A to C), Ki-RAS^{G12V}/$p53^{V143A}$-PDC were able to grow in an anchorage-independent manner and develop into large colonies (Fig. 3D and E). These results indicate that Ki-RAS^{G12V}/$p53^{V143A}$-PDC specifically acquired tumorigenic properties through the combination of Ki-*RAS* oncogene activation and *p53* tumor suppressor gene inactivation.

Furthermore, we wanted to assess the ability of the pancreatic ductal cells derived from different genotypes to form tumors in vivo. Stable expression of the firefly luciferase gene (*luc*) was obtained by retroviral transduction in WT-PDC, Ki-RAS^{G12V}-PDC, $p53^{V143A}$-PDC, and Ki-RAS^{G12V}/$p53^{V143A}$-PDC, and the luciferase activities from the cell lines were quantified (data not shown). WT/*luc*-PDC, Ki-RAS^{G12V}/*luc*-PDC, $p53^{V143A}$/*luc*-PDC, and Ki-RAS^{G12V}/$p53^{V143A}$-*luc*-PDC were subcutaneously injected into the dorsal flanks of irradiated immunodeficient mice. Then, over a 10-week period, tumor growth was monitored weekly according to both bioluminescence and tumor volume measurements. Importantly, tumors formed only in mice injected with Ki-RAS^{G12V}/$p53^{V143A}$*luc*-PDC. To investigate the linear correlation between tumor bioluminescence and tumor volume, we measured the bioluminescence activity at various stages of tumor development (Fig. 4A). At the conclusion of the observation period, all mice were euthanized, the tumors were excised, and bioluminescence was confirmed by ex vivo imaging (Fig. 4B and C). A second cohort of four mice were independently subcutaneously injected with Ki-RAS^{G12V}/$p53^{V143A}$-*luc*-PDC using the same conditions, except that the athymic mice were not irradiated, and all four mice developed subcutaneous tumors (data not shown). In aggregate from the independent experiments, the Ki-RAS^{G12V}/$p53^{V143A}$-*luc*-PDC yielded tumors in six of nine mice, and an additional two of the nine mice had weak bioluminescence activities corresponding to islands of tumor cells.

Sections of tissues isolated from mice injected with WT-PDC, Ki-RAS^{G12V}-PDC, and Ki-RAS^{G12V}/$p53^{V143A}$-PDC were evaluated by histology, and only Ki-RAS^{G12V}/$p53^{V143A}$-PDC developed into tumors, which were comprised of undifferentiated cells (Fig. 5A depicts two representative tumors). While immunohistochemical staining for the epithelial markers, cytokeratin and E-cadherin, was decreased but not abrogated, surprisingly, immunohistochemical staining for the mesenchymal markers vimentin and S-100 was positive in the tumor (Fig. 5A), which is compatible with the possibility of epithelial-mesenchymal transition (EMT). Furthermore, the majority of

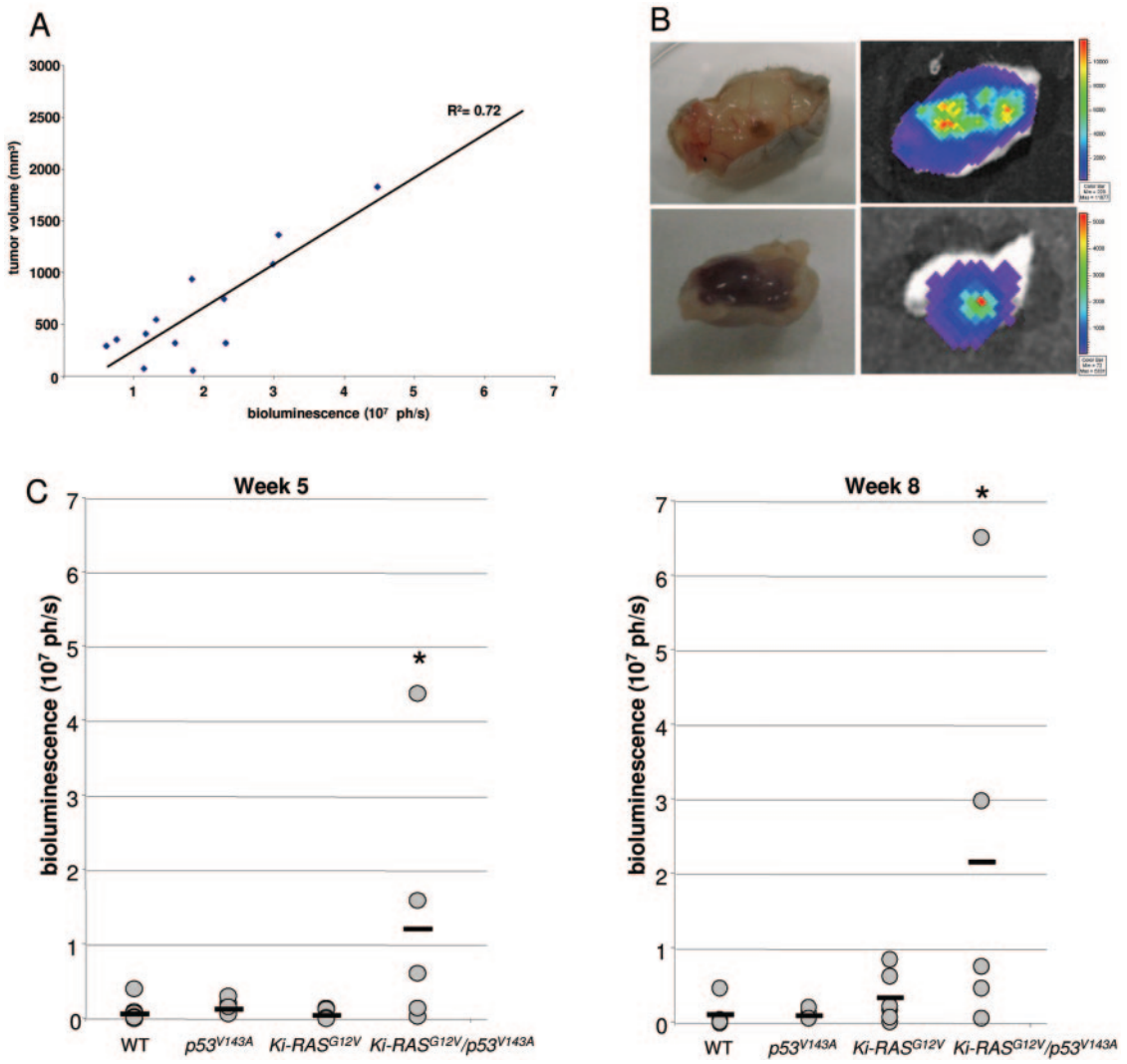

FIG. 4. In vivo bioluminescence imaging of WT-PDC, $p53^{V143A}$-PDC, Ki-RAS^{G12V}-PDC, and Ki-$RAS^{G12V}/p53^{V143A}$-PDC stably transduced with a pFB-neo/*luc* retroviral vector. Irradiated immunodeficient mice received subcutaneous injections of 1×10^7 cells suspended in a 1:1 ratio of Matrigel/DMEM/F12 full medium. Animals were imaged weekly for 10 weeks to monitor tumor growth. (A) Correlation between tumor volume (mm^3) and bioluminescence signal (photons per second [ph/s]) at various time points of tumor development in mice injected with WT-*luc*-PDC, $p53^{V143A}$-*luc*-PDC, Ki-RAS^{G12V}-*luc*-PDC, and Ki-$RAS^{G12V}/p53^{V143A}$-*luc*-PDC. Data are shown for individual mice at 1 to 8 weeks after subcutaneous injections ($R^2 = 0.72$). (B) After 10 weeks, ex vivo imaging of excised tumor tissues confirmed the presence of luciferase activity arising only from the Ki-$RAS^{G12V}/p53^{V143A}$-*luc*-PDC. Bioluminescence was measured 20 min after injection of the D-luciferin substrate. (C) Bioluminescence and growth of subcutaneous *luc*-PDC tumors are shown for week 5 and week 8 after subcutaneous injections of WT-*luc*-PDC ($n = 6$), $p53^{V143A}$-*luc*-PDC ($n = 6$), Ki-RAS^{G12V}-*luc*-PDC ($n = 7$), and Ki-$RAS^{G12V}/p53^{V143A}$-*luc*-PDC ($n = 5$), with a horizontal bar representing the mean value for each cell line. *n*, number of tumors considered for this experiment. *, *P* was <0.05 for Ki-$RAS^{G12V}/p53^{V143A}$-PDC versus WT-*luc*-PDC, $p53^{V143A}$-*luc*-PDC, or Ki-RAS^{G12V}-*luc*-PDC.

cells have evidence of p53 nuclear staining (data not shown), indicating stabilization of the p53 protein due to mutation ($p53^{V143A}$).

We demonstrated in independent experiments that the majority of mice formed subcutaneous tumors after being injected with Ki-$RAS^{G12V}/p53^{V143A}$-PDC. Yet the uptake rate was not 100%, and this may be due to differences in tumor kinetics, in part attributable to oxygen gradients in tumors and the degree of angiogenesis. Additionally, it is conceivable that the tendency to EMT fostered by Ki-$RAS^{G12V}/p53^{V143A}$ created a milieu permissive for tumor formation, and this may have been variable between mice implantations. Interestingly, in the case of the three genotypes in which tumors did not develop, the cells retained the capacity to form pancreatic ductal structures in vivo (data not shown).

In addition, a tumor cell line was established by processing subcutaneous tumors generated from one athymic mouse injected in four sites with Ki-$RAS^{G12V}/p53^{V143A}$-PDC. The colonies developing on collagen type I dishes showed heterogeneous phenotypes. Some colonies grew in a tight cell layer with strong cell-cell adhesion, while other colonies showed irregular cell morphology with decreased cell-cell adhesion and uneven colony borders (Fig. 5B). The tumor cells were selected with G418 for expression of luciferase and then subcutaneously

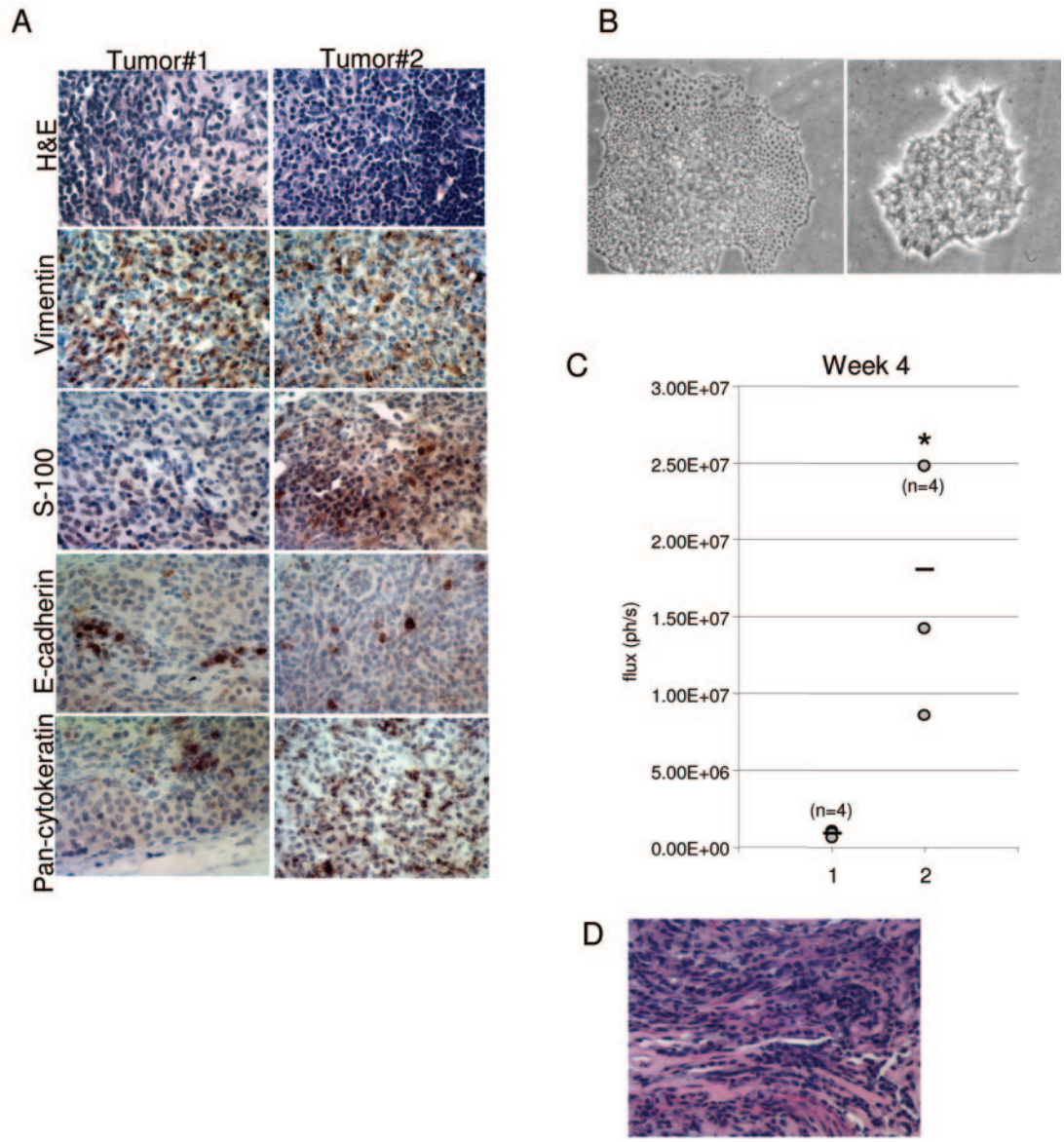

FIG. 5. Representative tumors isolated from immunodeficient mice injected with Ki-$RAS^{G12V}/p53^{V143A}$-PDC. (A) Hematoxylin and eosin (H&E) staining of two representative tumors (magnification, ×600). Positive staining in tumor cells of the mesenchymal markers, S-100 and vimentin, with reduced staining of the epithelial markers, pancytokeratin and E-cadherin. (B) Phase-contrast photomicrographs taken at ×40 magnification showing two types of colonies observed in cells isolated from Ki-$RAS^{G12V}/p53^{V143A}$-PDC subcutaneous tumors and grown on collagen type I. (C) Bioluminescence signals of subcutaneous tumor growth at week 4 after mice were injected with Ki-$RAS^{G12V}/p53^{V143A}$-*luc*-PDC (1) or tumor-derived cells (2). *n*, number of tumors studied for this experiment; ph/s, photons per second. *, *P* was <0.05 for bioluminescence activities in the subcutaneous tumors of tumor-derived cells versus Ki-$RAS^{G12V}/p53^{V143A}$-PDC. (D). H&E staining of subcutaneous tumor from tumor-derived $RAS^{G12V}/p53^{V143A}$-*luc*-PDC (magnification, ×600).

injected into recipient athymic nude mice. After tumor development was monitored weekly for 4 weeks, the bioluminescence signal quantification showed that mice injected with cells derived from the subcutaneous tumors developed tumors faster than mice that were injected with Ki-$RAS^{G12V}/p53^{V143A}$-PDC in the initial experiments (Fig. 5C).

Next, the Ki-$RAS^{G12V}/p53^{V143A}$-PDC were implanted orthotopically in the tails of the pancreases, and it was ensured that there was no leakage of cells into the peritoneal cavity. Bioluminescence measurements revealed that five out of six mice formed tumors in the pancreatic parenchyma at 5 weeks (Fig. 6), which was confirmed by MR imaging (Fig. 6), a powerful, high-resolution imaging modality (4, 12). The bioluminescence measurements revealed focal activities and were done with animals imaged using a left anterior oblique view to optimize imaging of the pancreatic tail. While no obvious metastatic disease was found within the time period tested, it is conceivable that overt metastatic disease would have been apparent had the mice been monitored for a prolonged period, which had to be tempered by potential illness due to the pancreatic tumors. Nevertheless, the temporal rate of tumor formation was more robust in orthotopic implantations compared to sub-

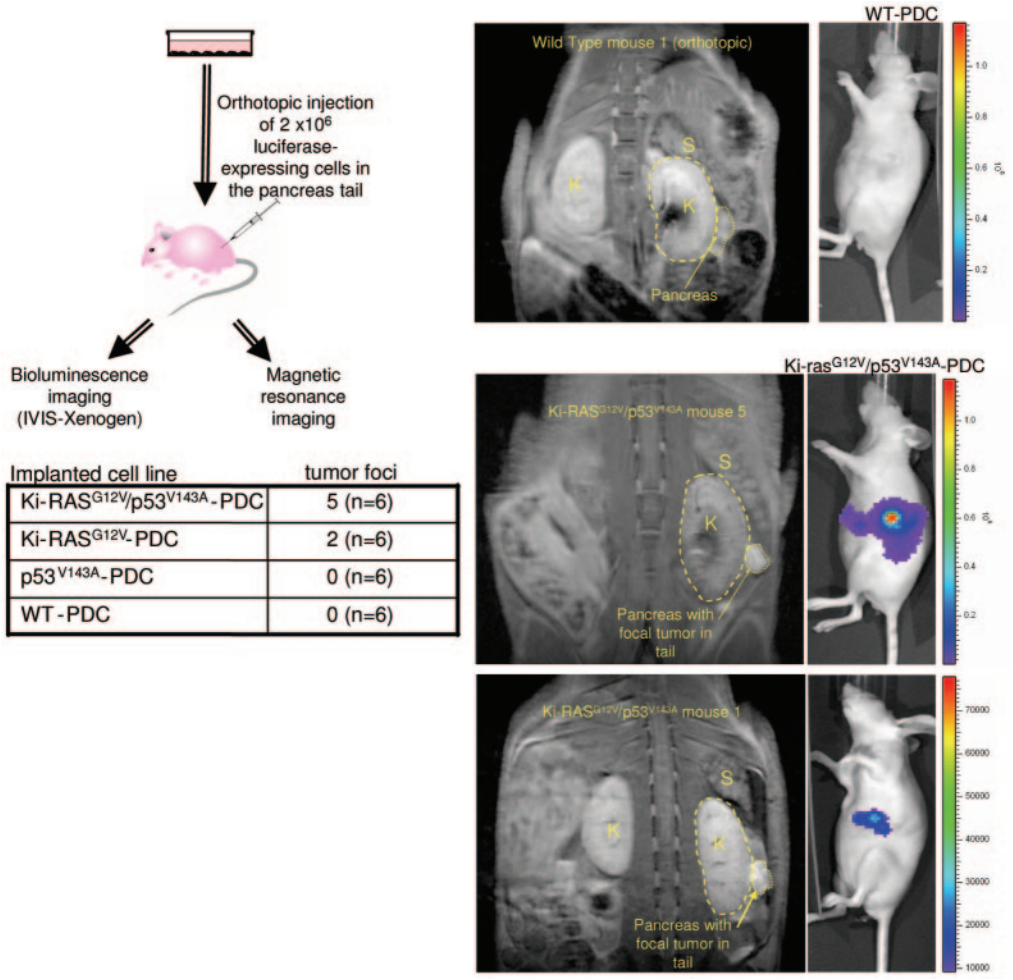

Implanted cell line	tumor foci
Ki-RAS^{G12V}/p53^{V143A}-PDC	5 (n=6)
Ki-RAS^{G12V}-PDC	2 (n=6)
p53^{V143A}-PDC	0 (n=6)
WT-PDC	0 (n=6)

FIG. 6. In vivo bioluminescence and MR imaging of immunodeficient mice injected orthotopically with Ki-*RAS*^{G12V}/*p53*^{V143A}-*luc*-PDC. WT-*luc*-PDC, *p53*^{V143A}-*luc*-PDC, Ki-*RAS*^{G12V}-*luc*-PDC, and Ki-*RAS*^{G12V}/*p53*^{V143A}-*luc*-PDC were injected deep into the pancreatic tails of six mice for each cell line ($n = 6$). Five weeks after implantation, bioluminescence was measured and MR imaging was performed. The number of mice presenting pancreatic focal tumors detectable by bioluminescence imaging is indicated in the table for each cell line. K, kidney; S, spleen.

cutaneous implantations, and only 10% of the number of cells used for subcutaneous implantations were used for orthotopic implantations, suggesting that the local milieu (e.g., soluble growth factors) might play a role in fostering tumor development and progression.

N-cadherin is induced in Ki-*RAS*^{G12V}-PDC but decreased in Ki-*RAS*^{G12V}/*p53*^{V143A}-PDC. To elucidate the influence of constitutive expression of mutant Ki-*RAS*^{G12V} in pancreatic ductal cells, gene microarrays were performed on WT-PDC, Ki-*RAS*^{G12V}-PDC, *p53*^{V143A}-PDC, and Ki-*RAS*^{G12V}/*p53*^{V143A}-PDC grown in two dimensions. After normalization of the microarray signal intensities, we identified 910 genes with a twofold or greater expression difference between Ki-*RAS*^{G12V}-PDC and WT-PDC (see the supplemental data at http://www.uphs.upenn.edu/abramson/supplementarymaterials.htm). Additional pairwise comparison analyses were done using a twofold cutoff between Ki-*RAS*^{G12V}/*p53*^{V143A}-PDC and Ki-*RAS*^{G12V}-PDC, Ki-*RAS*^{G12V}/*p53*^{V143A}-PDC and *p53*^{V143A}-PDC, and *p53*^{V143A}-PDC and WT-PDC (see the supplemental data at http://www.uphs.upenn.edu/abramson/supplementarymaterials.htm). These comparisons were also conducted for the three-dimensional spheroid cysts grown on Matrigel (see the supplemental data at http://www.uphs.upenn.edu/abramson/supplementarymaterials.htm).

Given the significance of cell migration and invasion, we focused upon the cadherins due to their importance in cell-cell homotypic and heterotypic interactions (Fig. 7A). Among the genes displaying greater than a twofold difference, we observed an increased (10.49-fold) expression of N-cadherin, which was also confirmed in the spheroid cysts. Interestingly, there was no difference in E-cadherin expression. We focused upon N-cadherin because of its established role in cell-cell adhesion and its role in tumorigenesis (1, 13, 18). RT-PCR and immunoblotting validated the results obtained in the gene array for N-cadherin (Fig. 7A and 8B). Furthermore, a 5.0-kb mouse N-cadherin promoter construct fused to the luciferase gene was transiently transfected into Ki-*RAS*^{G12V}-PDC and WT-PDC and found to be two to three times more active in Ki-*RAS*^{G12V}-PDC (data not shown). In WT-PDC, Ki-*RAS*^{G12V}-PDC, *p53*^{V143A}-PDC, and Ki-*RAS*^{G12V}/*p53*^{V143A}-PDC, N-cadherin is specifically lo-

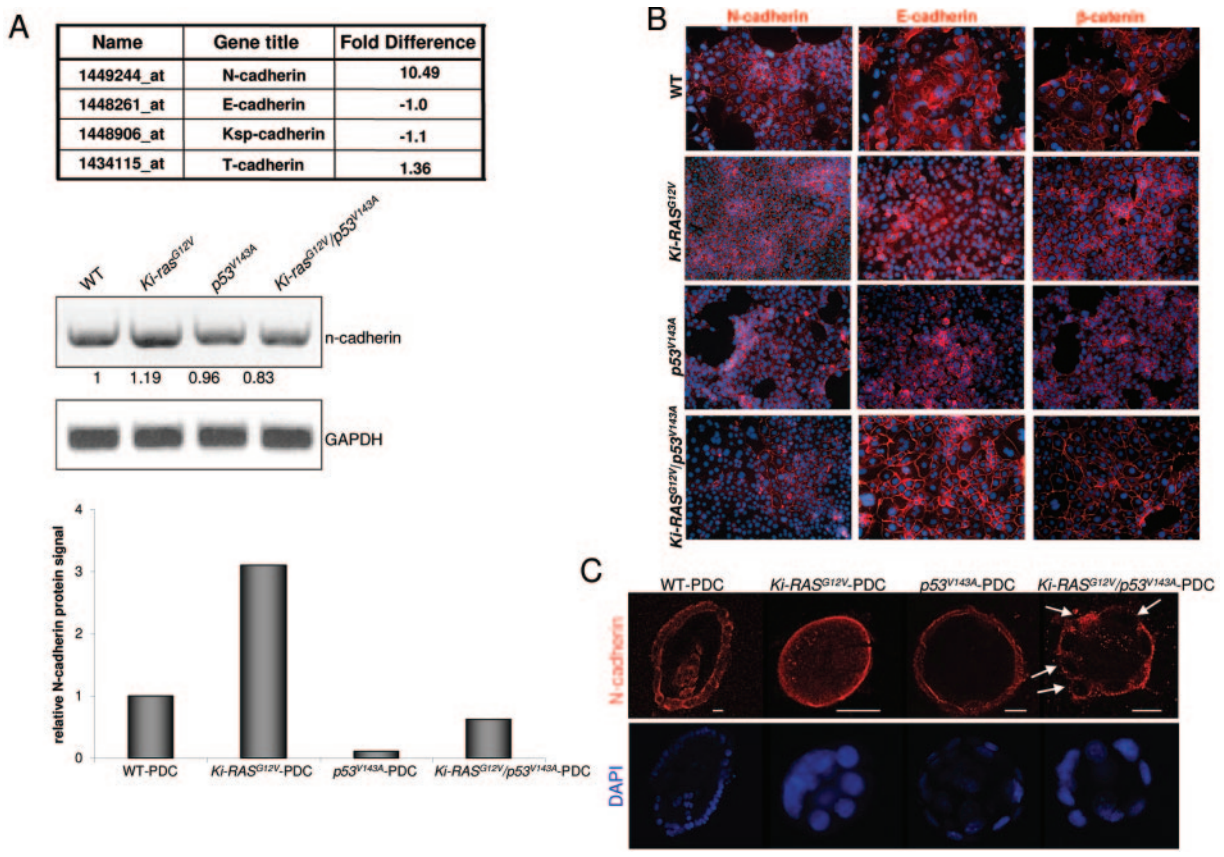

FIG. 7. Differential expression of N-cadherin in WT-PDC, $p53^{V143A}$-PDC, Ki-RAS^{G12V}-PDC, and Ki-$RAS^{G12V}/p53^{V143A}$-PDC. (A) Gene microarray results showing cadherin expression levels in Ki-RAS^{G12V}-PDC versus WT-PDC. Quantitative analysis of N-cadherin and β-actin transcript levels by RT-PCR and protein levels by Western blotting were assessed in WT-PDC, $p53^{V143A}$-PDC, Ki-RAS^{G12V}-PDC, and Ki-$RAS^{G12V}/p53^{V143A}$-PDC. These analyses are representative of several experiments. Densitometry of N-cadherin mRNA and protein levels was performed using Scion Image Beta 4.02 software (Frederick, MD) and calibrated with the β-actin signal. The N-cadherin protein level of WT-PDC was set at 1.0. (B) Indirect immunofluorescence of N-cadherin (red), E-cadherin (red), and β-catenin (red) in PDC grown in a monolayer. Nuclei were counterstained with DAPI (blue). Magnification, ×400. (C) Indirect immunofluorescence of N-cadherin (red) and nuclei (blue) in PDC cysts grown in type I collagen. Arrows indicate partial loss of N-cadherin in Ki-$RAS^{G12V}/p53^{V143A}$-PDC. Scale bar = 20 μm. Magnification, ×250.

calized to the cell membrane based upon immunofluorescence (Fig. 7B), but its expression is decreased in Ki-$RAS^{G12V}/p53^{V143A}$-PDC. E-cadherin protein levels are not altered, as confirmed by immunofluorescence (Fig. 7B) and Western blotting (data not shown). β-Catenin is predominantly membrane associated (Fig. 7B), suggesting that nuclear translocation of β-catenin is not observed with the introduction of $p53^{V143A}$ into Ki-RAS^{G12V}-PDC. Immunofluorescence staining by confocal microscopy of N-cadherin reveals that the areas of greatest disruption in cellular architecture in Ki-$RAS^{G12V}/p53^{V143A}$-PDC spheroid cysts are associated with loss of N-cadherin and, in rare instances, with cytoplasmic localization of N-cadherin, presumably rendering N-cadherin nonfunctional (Fig. 7C). Interestingly, E-cadherin levels are preserved, and its localization remains membranous (Fig. 2).

Association of N-cadherin with KGFR and N-CAM in pancreatic ductal cells. FGFRs have been shown previously to be overexpressed in a subset of human pancreatic cancers and derived cell lines (29, 32, 33). N-CAM forms a multiprotein complex comprising FGFR-4 and N-cadherin, activating signal transduction pathways that lead to increased cell-cell adhesion, thereby potentially preventing the dissemination of metastatic tumor cells (16). By contrast, Suyama et al. have suggested that the interaction of N-cadherin with FGFR-1 resulted in sustained MAPK–extracellular signal-regulated kinase activation and cellular invasiveness (47). Thus, we sought to investigate potential interactions between N-CAM and FGFRs in the various pancreatic ductal genotypes.

Analysis of the gene microarray data shows a significant decrease of N-CAM and FGFR-2 expression levels in Ki-$RAS^{G12V}/p53^{V143A}$-PDC (Fig. 8A), which was also confirmed in three-dimensional spheroid cysts (data not shown). Western blotting showed that WT-PDC, Ki-RAS^{G12V}-PDC, $p53^{V143A}$-PDC, and Ki-$RAS^{G12V}/p53^{V143A}$-PDC express N-cadherin, N-CAM, and FGFR-2, while expression of these is decreased in $p53^{V143A}$-PDC and Ki-$RAS^{G12V}/p53^{V143A}$-PDC (Fig. 8B). We demonstrated that N-cadherin is immunoprecipitated specifically with FGFR-2 and N-CAM (Fig. 8C) but not with FGFR-3 (data not shown), which is also expressed in mouse pancreatic ductal cells. N-cadherin is known to bind FGFR through the former's first two extracellular Ig-like domains. Notably, FGFR-1 and FGFR-4 are not expressed in any of the pancreatic ductal cells (data not shown).

Since FGFR-2 has two isoforms, designated IIIb and IIIc, we

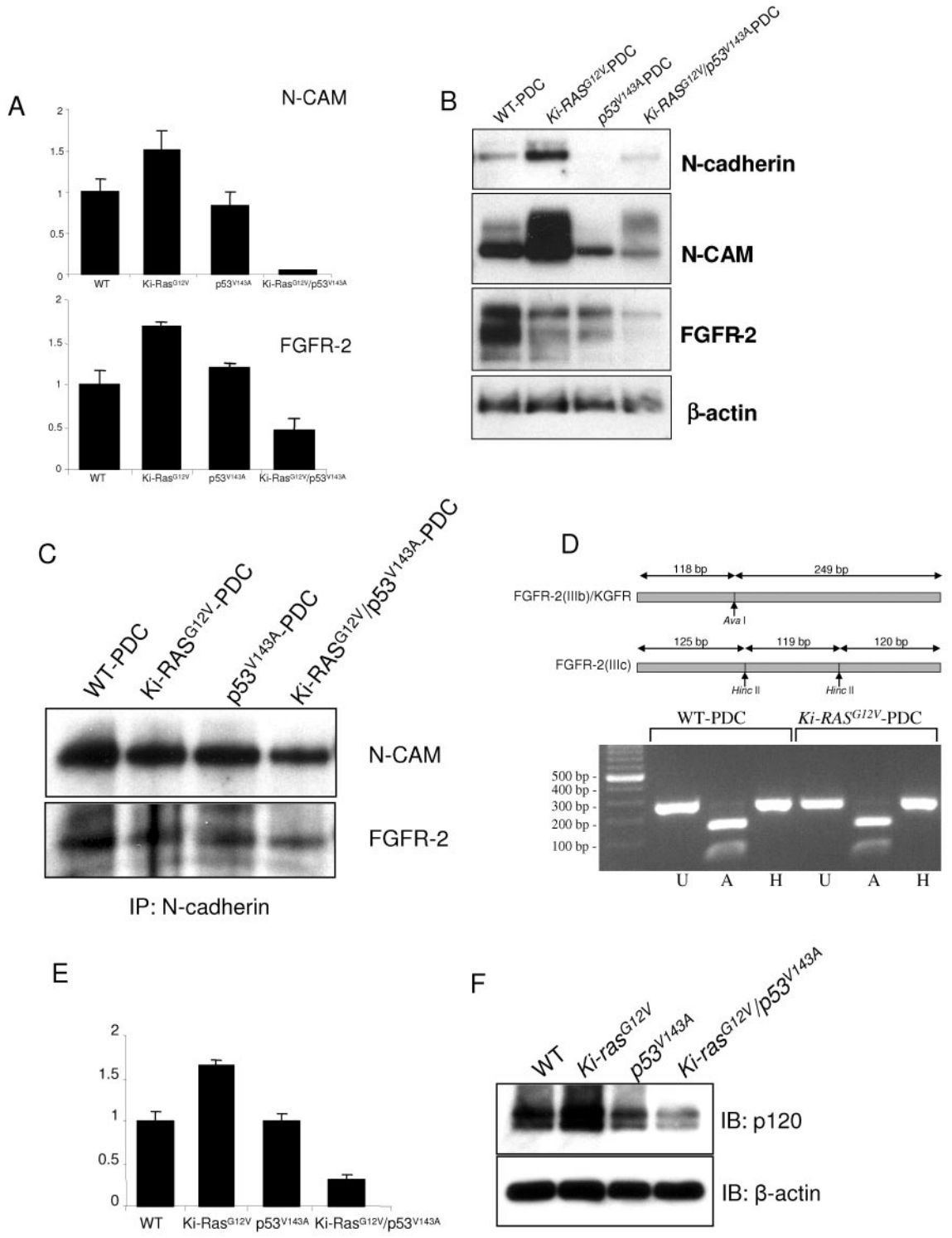

FIG. 8. KGFR is the FGFR-specific isoform that associates with N-cadherin and N-CAM. (A) Gene microarray results showing N-CAM and FGFR-2 transcript levels in WT-PDC, *p53*^{V143A}-PDC, Ki-*RAS*^{G12V}-PDC, and Ki-*RAS*^{G12V}/*p53*^{V143A}-PDC, with transcript levels in WT-PDC set at 1.0. (B) Western blots show N-cadherin, N-CAM, and FGFR-2 protein expression in the PDC and confirm the microarray results. (C) Immunoprecipitation (IP) of N-cadherin followed by immunoblotting for N-CAM and FGFR-2. (D) Alternative splicing of FGFR-2. Amplification of the FGFR-2-specific PCR product followed by digestion with restriction enzymes determined which FGFR-2 isoform is expressed in the PDC. FGFR-2 PCR products amplified from WT-PDC and Ki-*RAS*^{G12V}-PDC are digested with AvaI only, suggesting that FGFR-2(IIIb) or KGFR is the only isoform expressed in the PDC. U, undigested PCR products; A and H, PCR products digested with restriction enconucleases AvaI and HincII, respectively. (E) Gene microarray results of p120-catenin transcript levels in WT-PDC, *p53*^{V143A}-PDC, Ki-*RAS*^{G12V}-PDC, and Ki-*RAS*^{G12V}/*p53*^{V143A}-PDC, with expression of WT-PDC set at 1.0. (F) Western blotting (IB) for p120-catenin in the PDC confirms the microarray results.

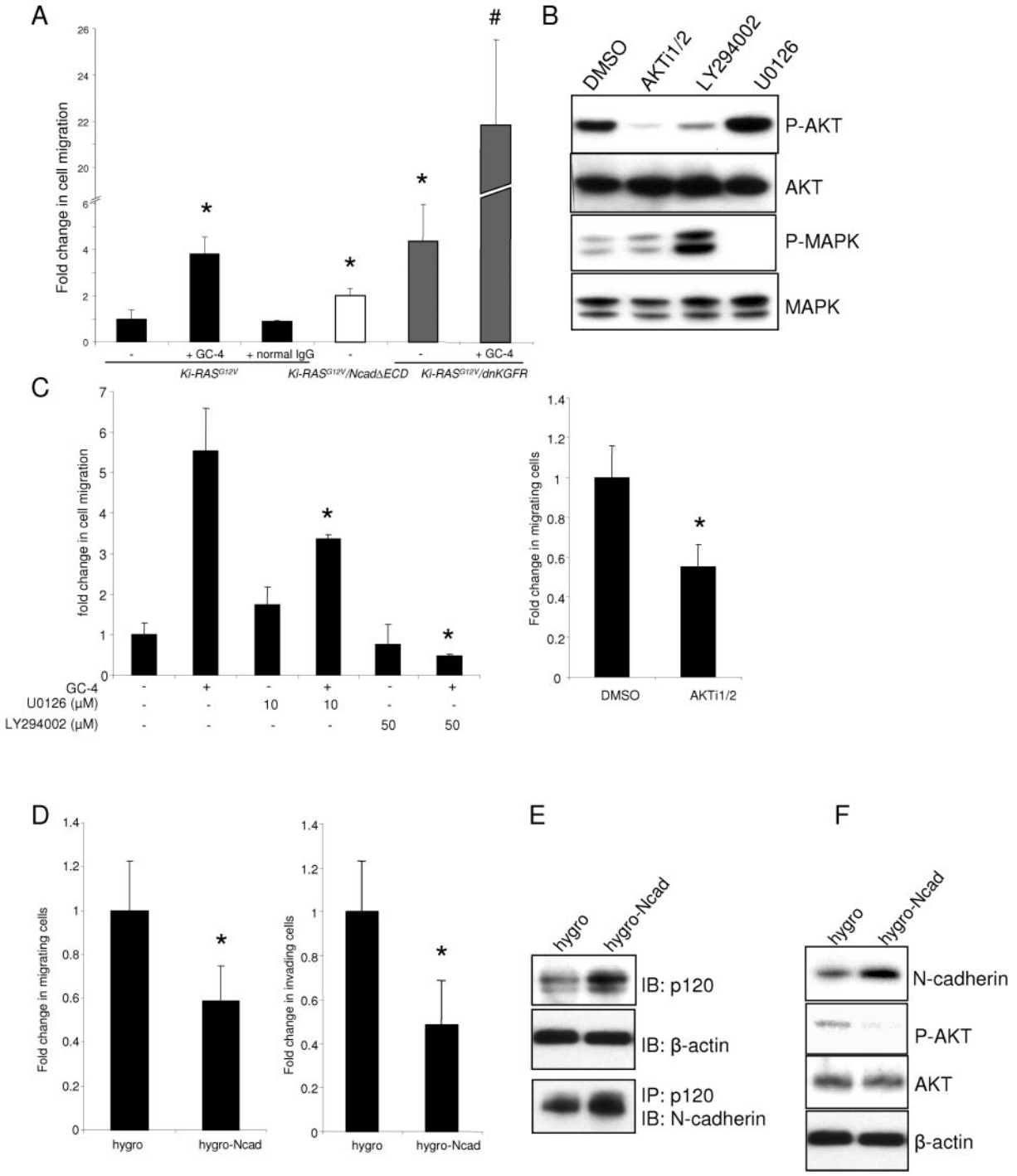

FIG. 9. Disruption of the N-cadherin/KGFR/N-CAM complex in Ki-*RAS*^{G12V}-PDC leads to an increase in cell migration. (A) Ki-*RAS*^{G12V}-PDC were preincubated with the N-cadherin-neutralizing antibody GC-4 or control IgG for 20 min prior to migration assays. Ki-*RAS*^{G12V}/*NcadΔECD*-PDC and Ki-*RAS*^{G12V}/*dnKGFR*-PDC demonstrated an increase in migration compared to Ki-*RAS*^{G12V}-PDC. A synergistic increase in cell migration was observed in Ki-*RAS*^{G12V}/*dnKGFR*-PDC pretreated with GC-4. *, P was <0.02 for Ki-*RAS*^{G12V}-PDC treated with GC-4, Ki-*RAS*^{G12V}/*NcadΔECD*-PDC, and Ki-*RAS*^{G12V}/*dnKGFR*-PDC versus the Ki-*RAS*^{G12V}-PDC control. #, P was <0.0001 for GC-4-treated versus untreated Ki-*RAS*^{G12V}/*dnKGFR*-PDC. (B) Western blotting demonstrates the effects of specific inhibitors on AKT phosphorylation (P-AKT) and extracellular signal-regulated kinase 1/2 phosphorylation (P-MAPK). Ki-*RAS*^{G12V}-PDC were incubated in the presence of 10 μM AKT specific inhibitor (AKTi1/2), 50 μM PI3K inhibitor (LY294002), or 10 μM MEK1/2 inhibitor (U0126) for 24 h. DMSO, dimethyl sulfoxide. (C and D) Migrating or invading cells were stained and quantified after 24 h. The data shown are expressed as means ± standard deviations of 10 individual fields from at least two independent experiments performed in duplicate. (C) Ki-*RAS*^{G12V}-PDC were incubated in the presence or absence of 10 μM U0126, 50 μM LY294002, or 10 μM AKTi1/2 for the duration of the migration assay. N-cadherin-neutralizing antibody GC-4-dependent migration was decreased partially by U0126 and robustly by LY294002. ANOVA was used to compare AKTi1/2-treated to untreated Ki-*RAS*^{G12V}-PDC (*, $P <$ 0.002). (D) Ectopic expression of full-length N-cadherin in Ki-*RAS*^{G12V}/*p53*^{V143A}-PDC (hygro-Ncad) decreased cell migration and invasion

wished to determine which isoform may be specifically or preferentially expressed in pancreatic ductal cells. Using a PCR-based strategy, the products resulting from RT-PCR with specific primers for FGFR-2 were digested with AvaI or HincII restriction enzyme (15). Digestion by AvaI alone indicates that the isoform FGFR-2(IIIb) is specifically expressed in the pancreatic ductal cells and the FGFR-2(IIIc) isoform is not expressed (Fig. 8D). FGFR-2(IIIb) is also referred to as KGFR and is activated through binding with cognate ligands of the FGF family. Thus, we show for the first time that N-cadherin binds specifically to FGFR-2(IIIb) or KGFR and to N-CAM in pancreatic ductal cells.

Next we wished to determine whether p120-catenin may be differentially bound to N-cadherin. Microarray data (Fig. 8E) and Western blotting (Fig. 8F) reveal that p120-catenin is downregulated in Ki-$RAS^{G12V}/p53^{V143A}$-PDC, corresponding to decreased N-cadherin levels in these cells. The microarray data for p120-catenin in the different genotypes were also confirmed in microarrays from the three-dimensional spheroid cysts (see the supplemental data at http://www.uphs.upenn.edu/abramson/supplementarymaterials.htm).

Ki-*RAS* and *p53* regulate N-cadherin to influence cell migration and invasion. To investigate further the role played by N-cadherin in pancreatic ductal cellular processes of migration and invasion, we used complementary pharmacological and genetic approaches to inhibit N-cadherin or KGFR, thereby mimicking the effects of Ki-$RAS^{G12V}/p53^{V143A}$-PDC in which N-cadherin is downregulated. We derived Ki-RAS^{G12V}/*Ncad*Δ*ECD*-PDC (retrovirally transduced to stably express mutant N-cadherin containing the deletion of its extracellular domains) and Ki-RAS^{G12V}/*dnKGFR*-PDC (retrovirally transduced to stably express a dominant negative version of KGFR). Upon treatment of Ki-RAS^{G12V}-PDC with an N-cadherin-neutralizing antibody (designated GC-4), a 3.5-fold increase in cell migration compared to untreated cells was observed (Fig. 9A). Similarly, Ki-RAS^{G12V}-PDC expressing *Ncad*Δ*ECD* or *dnKGFR* migrated significantly more than Ki-RAS^{G12V}-PDC (Fig. 9A). Interestingly, the combination of the N-cadherin-neutralizing antibody and dnKGFR has an apparent synergistic effect in augmenting cell migration more than fivefold compared to dnKGFR alone (Fig. 9A). Importantly, these effects are recapitulated in Ki-$RAS^{G12V}/p53^{V143A}$-PDC, where there is a downregulation of N-cadherin (data not shown). In aggregate, the downregulation of either N-cadherin or KGFR or the combination is important to mediate the enhanced cell migration that is a property of tumor cells. As a related functional outcome, treatment of Ki-RAS^{G12V}-PDC with N-cadherin-neutralizing antibody results in increased invasion, reminiscent of what is observed in Ki-$RAS^{G12V}/p53^{V143A}$-PDC in which N-cadherin is downregulated (data not shown).

Migration and invasion are mediated in part through disruption of the adherens junctions and AKT activation. To determine which downstream signaling pathway(s) is activated during migration, we undertook complementary, comprehensive pharmacological and genetic approaches. Pancreatic ductal cells were treated with the PI3K inhibitor LY294002, the AKT specific inhibitor AKTi1/2, and the MEK1/2 inhibitor U0126. We first confirmed their specificities by demonstrating effects on the phosphorylation of their cognate substrates (Fig. 9B). Treatment of Ki-RAS^{G12V}-PDC with LY294002 attenuated cell migration (Fig. 9C) and invasion (data not shown) in Ki-RAS^{G12V}-PDC (Fig. 9C) and also in WT-PDC, $p53^{V143A}$-PDC, and Ki-$RAS^{G12V}/p53^{V143A}$-PDC (data not shown), which was most apparent when the PDC had undergone inactivation of N-cadherin with the N-cadherin-neutralizing antibody (GC-4), suggesting that the initial event of N-cadherin inactivation precedes downstream activation of AKT. In addition, cell migration was attenuated following AKTi1/2 treatment, a more specific AKT inhibitor (Fig. 9C). Treatment with U0126 also inhibited cell migration (Fig. 9C) and invasion (data not shown) in Ki-RAS^{G12V}-PDC upon treatment with GC-4, albeit to a lesser extent (Fig. 9C) compared to PI3K treatment. This pattern was also apparent in the other genotypes (data not shown). In order to determine whether restoration of N-cadherin in Ki-$RAS^{G12V}/p53^{V143A}$-PDC might rescue the enhanced migratory and invasive phenotype of these cells, N-cadherin was retrovirally transduced into Ki-$RAS^{G12V}/p53^{V143A}$-PDC, resulting in an induction of N-cadherin at a level similar to that observed in Ki-RAS^{G12V}-PDC and leading to a statistically significant decrease in cell migration and invasion (Fig. 9D). Furthermore, the restoration of N-cadherin in the Ki-$RAS^{G12V}/p53^{V143A}$-PDC resulted in an augmented p120-catenin level (as shown in Fig. 8E and F) with greater interaction between N-cadherin and p120-catenin (Fig. 9E) and suppression of phosphorylated AKT (Fig. 9F). Taken together, we surmise that modulation of N-cadherin level in both two-dimensional and three-dimensional cultures, and perhaps changes in subcellular localization as well, lead to differential recruitment of p120-catenin. While the N-cadherin-p120-catenin interaction is preserved, there is nevertheless diminished interaction, thereby suggesting that the adherens junction is more apt to be disrupted in Ki-$RAS^{G12V}/p53^{V143A}$-PDC. This is a prerequisite for initiating cell migration and invasion, which in part is triggered through activation of AKT, although activation of MAPK plays a role as well, and other pathways are not necessarily excluded.

DISCUSSION

In the present study, we sought to determine the mechanistic underpinnings of p53 mutation in combination with Ki-*RAS* mutation in promoting pancreatic cancer. We found that introduction of the $p53^{V143A}$ gene into Ki-RAS^{G12V}-PDC led to the rapid acquisition of a transformed phenotype as indicated

compared to control Ki-$RAS^{G12V}/p53^{V143A}$-PDC (hygro). ANOVA was used to compare Ki-$RAS^{G12V}/p53^{V143A}$-PDC expressing full-length N-cadherin or control hygro (*, $P < 0.04$). (E) N-cadherin-expressing Ki-$RAS^{G12V}/p53^{V143A}$-PDC (hygro-Ncad) demonstrate an increase in p120-catenin expression compared to control hygro. Immunoprecipitation (IP) for p120-catenin was followed by immunoblotting (IB) for N-cadherin. (F) Western blot shows that increased N-cadherin expression is accompanied by a decrease in activated or phosphorylated AKT, consistent with the inhibition of AKT shown in panel C.

by the ability of $p53^{V143A}$-infected cells to form colonies in soft agar, exhibit increased cell migration and invasiveness, display loss of epithelial polarity and disrupted tissue architecture in three-dimensional culture, and foster tumor formation in immunodeficient mice, in cases of both subcutaneous and pancreatic orthotopic implantations, the latter of which were monitored by bioluminescence and magnetic resonance imaging. Furthermore, we have demonstrated that modulation of N-cadherin by Ki-RAS^{G12V} and *p53* is critical in part in mediating cell migration and invasion.

Cross talk between tumor cells and stromal cells influences tumor development and progression. Cadherins represent a family of cell surface glycoproteins that promote homotypic and heterotypic cell-cell adhesion and constitute the transmembrane components of cell-cell adherens (49). Classic cadherins, namely E-, N-, and P-cadherins, are expressed in specific temporal and spatial patterns. Epithelial cells are joined by adherens junctions, which consist of homotypic interactions between extracellular domains of E-cadherins. Inside the cell, the tails of cadherins bind actin cables through β-catenin and α-catenin. Cadherins regulate adhesion and motility with dynamic rearrangements of the actin cytoskeleton.

N-cadherin is mainly expressed in neurons, muscle cells, and mesenchymal cells, although it can be expressed in epithelial cells. During pancreatic development, N-cadherin-deficient mice suffer from selective agenesis of the dorsal pancreas, involving an essential function of N-cadherin as a survival factor in the dorsal pancreatic mesenchyme (20). N-cadherin is a critical adhesion molecule whose function is modulated by protein-protein interactions and phosphorylation/dephosphorylation events.

Our results indicate that N-cadherin mediates adhesion between pancreatic ductal cells. This facilitates dynamic cellular processes such as migration and invasion. In particular, downregulation of N-cadherin, which was achieved through complementary means, namely the use of a neutralizing antibody, stable retroviral transduction of a dominant negative mutant (deletion of the cytoplasmic tail) of N-cadherin, or introduction of mutant p53, all of which promote enhanced pancreatic ductal cell migration and invasion. Microarray data, corroborated by RT-PCR and Western blotting, revealed that N-cadherin is upregulated with the introduction of Ki-RAS^{G12V} into WT-PDC and subsequently downregulated with the introduction of $p53^{V143A}$ into Ki-RAS^{G12V}-PDC or WT-PDC. The induction of N-cadherin appears to be mediated through the induction of the N-cadherin promoter (data not shown).

Migration and invasion may be further fostered by changes in the cellular-extracellular matrix (ECM) interactions through modifications in structural components within the cell and in the matrix. To that end, modulation of N-cadherin results in the differential recruitment of p120-catenin. First, microarray data revealed that p120-catenin is upregulated in Ki-RAS^{G12V}-PDC but downregulated in $p53^{V143A}$-PDC and is even more downregulated in Ki-RAS^{G12V}/$p53^{V143A}$-PDC. Western blotting demonstrated a coordinated increase in N-cadherin and p120-catenin in Ki-RAS^{G12V}-PDC but a coordinated decrease of both N-cadherin and p120-catenin in $p53^{V143A}$-PDC and in Ki-RAS^{G12V}/$p53^{V143A}$-PDC. While the physical interaction between N-cadherin and p120-catenin remains intact in all the genotypes, there is less detectable interaction in $p53^{V143A}$-PDC and in Ki-RAS^{G12V}/$p53^{V143A}$-PDC. This would suggest that there is less formation of adherens junctions in $p53^{V143A}$-PDC and in Ki-RAS^{G12V}/$p53^{V143A}$-PDC, which would appear to be a requirement for cells to initiate migration. Indeed, we do observe fewer adherens junctions in cells from both genotypes, and that is the case much more so in Ki-RAS^{G12V}/$p53^{V143A}$-PDC both in two-dimensional and three-dimensional cultures. We cannot exclude the possibility that N-cadherin-independent mechanisms contribute to PDC migration and invasion and that $p53^{V143A}$ may function in a manner(s) independent of the combinatorial effects that we observe between $p53^{V143A}$ and Ki-RAS^{G12V}. Nevertheless, N-cadherin's role appears to be important and directly underscored by the retroviral transduction of N-cadherin into Ki-RAS^{G12V}/$p53^{V143A}$-PDC and greater recruitment of p120-catenin, with a resulting attenuation in both migration and invasion in these tumorigenic cells. p120-catenin may affect the activity of Rho family GTPases (6, 7, 39). Changes in N-cadherin and shifts in p120-catenin could influence the equilibrium between p120-catenin and Rho family GTPases and thus affect ultimate cell migration and invasion.

It has been previously demonstrated that loss of N-cadherin in neural crest cells and endothelial cells leads to faster migration and loss of directionality (36, 57). The level of N-cadherin and its ability to regulate migration and invasion may be further influenced by the particular cell type and tissue context (25). It is interesting to note that in our system N-cadherin is regulatable by Ras and p53, but E-cadherin levels and localization remain constant and do not make any obvious initial contribution, which has been observed also in breast cancer cells (38). Thus, the canonical reciprocal relationship between N-cadherin and E-cadherin in promoting cell migration is not always apparent; rather, N-cadherin may be regulatable and E-cadherin levels may remain constant in certain cellular and tissue contexts.

Can N-cadherin be regulated through interaction with other proteins, apart from p120-catenin? The family of FGFs are expressed ubiquitously and involved in embryonic development and diverse cellular functions, such as proliferation, differentiation, and migration (10). FGFs have also been implicated in tumor progression and metastasis. They bind tyrosine kinase receptors (FGFRs) and the heparan sulfate proteoglycans. Over 20 FGF homologues have been identified. FGFR-1 deletions (32) and FGFR-3 overexpression (33) have been shown to be present in human pancreatic adenocarcinomas, although the functional consequences of these events have not been elucidated. We found that KGF specifically elicited activation of KGFR, also known as FGFR-2(IIIb), with subsequent activation of FGFR substrate 2 (data not shown). We also found that a dominant negative version of KGFR augments basal migration in a manner similar to abrogation of N-cadherin function. The abrogation of both N-cadherin and KGFR results in a synergistic enhancement of migration. Our results are the first, to our knowledge, to demonstrate the importance of KGFR or FGFR-2(IIIb) in pancreatic cancer. It has been previously shown that tumor-ECM adhesion is facilitated by the interaction between N-CAM and FGFR-4 in beta cells of the pancreas (16). This ECM adhesion is inhibited by N-CAM deletion or a dominant negative form of FGFR-4. N-cadherin's EC4 extracellular domain interacts with FGFR-1's D1 and D2 extracellular domains upon engagement of

FGFR-1 by the FGF2 ligand (47), which then stimulates MAP kinase to induce MMP-9 gene transcription and cellular invasion by breast cancer cells. The type of FGFR isoform involved in the N-cadherin/N-CAM complex may be dependent upon the particular cell and tissue type (16, 31). Furthermore, the interaction of N-cadherin's extracellular domain with the heparin binding domain of FGFR-1 is believed to activate a signaling pathway that culminates in neurite outgrowth (19). Our microarray data for both two-dimensional and in three-dimensional cell culture systems indicate downregulation of N-CAM and KGFR in Ki-$RAS^{G12V}/p53^{V143A}$-PDC, although a comparable extent of downregulation is shown by Western blotting in both $p53^{V143A}$-PDC and Ki-$RAS^{G12V}/p53^{V143A}$-PDC. While the physical interaction between N-cadherin, NCAM, and KGFR is preserved, it is conceivable that this affects the extent of p120-catenin recruitment of N-cadherin and/or triggers different signaling cascades.

What signaling pathway(s) is induced through the differential regulation of N-cadherin in the different genotypes? Integrin-mediated cell adhesion and migration is often coordinated with cadherin-based cell-cell adhesion. Focal adhesion kinase has been implicated as a mediator of cell migration, typically as a positive regulator (42, 43), although recently it was found to be a negative regulator (58). In this context, the type of migration test may be important. On collagen, cells treated with FAK and paxillin small interfering RNAs demonstrate smaller focal adhesions and a protrusive morphology (58), which is different from $fak^{-/-}$ and $paxillin^{-/-}$ fibroblasts where fibronectin is typically used as a substrate for adhesion (24, 28). Our results suggest that phosphorylation of AKT contributes to migration in the PDC. This is demonstrated through the inhibition of PI3K and direct inhibition of AKT, and perhaps the most direct evidence is with the restoration of N-cadherin in Ki-$RAS^{G12V}/p53^{V143A}$-PDC with attenuation of migration and invasion that is accompanied by suppression of activated or phosphorylated AKT. It is possible that this leads to alterations in FAK phosphorylation and integrin-mediated interaction with components of the extracellular matrix. We do not claim that activation of AKT is the sole mediator of migration in PDC, since inhibition of MAPK does partially inhibit migration of Ki-RAS^{G12V}-PDC. Nevertheless, the involvement of more than the signaling cascade in regulating cell migration and invasion would not be surprising and is apparent in mammalian cells.

The intrinsic advantages of three-dimensional cell culture systems are that cell adhesion-dependent tissue architecture, homotypic cell-cell interactions, and tissue differentiation can be recapitulated, and that cellular behavior can be studied in a dynamic fashion (17, 59). Cell-ECM interactions drive tissue organization through dynamic and coordinated regulation of homotypic cell-cell interactions. A property of three-dimensional epithelial tissue architecture in vitro is polarity, and polarity is essential for tissue function (54, 60). Disruption of homotypic and heterotypic cellular interactions by activated Ki-RAS and inactivated p53 in our model helps to explain how the microenvironment can influence growth, migration, and invasion. The robustness of the three-dimensional cell culture system is underscored further by the nearly identical microarray results for N-cadherin, p120-catenin, N-CAM, and KGFR observed in both two-dimensional and three-dimensional cell culture systems. The loss of polarity is evident not only in our three-dimensional cell culture system but also in the xenotransplantation model, in which EMT is an important step during pancreatic cancer invasion and the accompanying desmoplastic response (22, 25, 30). The combination of activated oncogenic Ki-RAS and inactivated p53 promotes tumorigenicity in several different manners, as revealed in soft agar assays, three-dimensional cell culture, and xenotransplantation experiments. While subcutaneous and pancreatic orthotopic tumors form after injection of Ki-$RAS^{G12V}/p53^{V143A}$-PDC, and the uptake rate is shown to be even greater with transfer of tumor cells from donor mouse to recipient mouse, we cannot exclude the involvement of other factors in the initiation and progression of pancreatic tumorigenesis, including those derived from the epithelial and stromal compartments. Nonetheless, we believe that the initial steps instigated by Ki-RAS and p53 during pancreatic carcinogenesis are disruption of epithelial cell polarity and concordant deadhesion, which promote subsequent migration and invasion. These new insights may provide a basis for targeted therapeutic strategies.

ACKNOWLEDGMENTS

This work was supported by NIH/NIDDK grant R01 DK50306 (A.K.R., T.B.D., M.T., M.J.B., and B.R.), the National Pancreas Foundation (T.B.D.), NIH grants RO1-EB001872 and R24-CA92782 (U.M., R.U., and R.W.), the NIH/NIDDK Center for Molecular Studies in Digestive and Liver Diseases (Morphology, Molecular Biology, Mouse, and Cell Culture Cores) grant P30 DK50306, and the Bioluminescence Molecular Imaging Core facility at the University of Pennsylvania (supported in part by NIH grant CA105008).

We thank Gary Swain, Kelly Dempsey, and Shukriyyah Mitchell for technical assistance, Eric Bernhard for assistance with radiation experiments, Russ Carstens and Wafik El-Deiry for reagents, and members of the Rustgi laboratory (Hiroshi Nakagawa, Hideki Harada, Claudia Andl, and Takaomi Okawa) for discussion.

REFERENCES

1. **Agbunag, C., and D. Bar-Sagi.** 2004. Oncogenic K-ras drives cell cycle progression and phenotypic conversion of primary pancreatic duct epithelial cells. Cancer Res. **64:**5659–5663.
2. **Aguirre, A. J., N. Bardeesy, M. Sinha, L. Lopez, D. A. Tuveson, J. Horner, M. S. Redston, and R. A. DePinho.** 2003. Activated Kras and Ink4a/Arf deficiency cooperate to produce metastatic pancreatic ductal adenocarcinoma. Genes Dev. **17:**3112–3126.
3. **Aguirre, A. J., C. Brennan, G. Bailey, R. Sinha, B. Feng, C. Leo, Y. Zhang, J. Zhang, J. D. Gans, N. Bardeesy, C. Cauwels, C. Cordon-Cardo, M. S. Redston, R. A. DePinho, and L. Chin.** 2004. High-resolution characterization of the pancreatic adenocarcinoma genome. Proc. Natl. Acad. Sci. USA **101:**9067–9072.
4. **Alencar, H., R. King, M. Funovics, C. Stout, R. Weissleder, and U. Mahmood.** 2005. A novel mouse model for segmental orthotopic colon cancer. Int. J. Cancer **117:**335–339.
5. **Almoguera, C., D. Shibata, K. Forrester, J. Martin, N. Arnheim, and M. Perucho.** 1988. Most human carcinomas of the exocrine pancreas contain mutant c-K-ras genes. Cell **53:**549–554.
6. **Anastasiadis, P. Z., S. Y. Moon, M. A. Thoreson, D. J. Mariner, H. C. Crawford, Y. Zheng, and A. B. Reynolds.** 2000. Inhibition of RhoA by p120 catenin. Nat. Cell Biol. **2:**637–644.
7. **Anastasiadis, P. Z., and A. B. Reynolds.** 2001. Regulation of Rho GTPases by p120-catenin. Curr. Opin. Cell Biol. **13:**604–610.
8. **Andl, C. D., T. Mizushima, H. Nakagawa, K. Oyama, H. Harada, K. Chruma, M. Herlyn, and A. K. Rustgi.** 2003. Epidermal growth factor receptor mediates increased cell proliferation, migration, and aggregation in esophageal keratinocytes in vitro and in vivo. J. Biol. Chem. **278:**1824–1830.
9. **Behrens, J., M. M. Mareel, F. M. Van Roy, and W. Birchmeier.** 1989. Dissecting tumor cell invasion: epithelial cells acquire invasive properties after the loss of uvomorulin-mediated cell-cell adhesion. J. Cell Biol. **108:** 2435–2447.
10. **Boilly, B., A. S. Vercoutter-Edouart, H. Hondermarck, V. Nurcombe, and X. Le Bourhis.** 2000. FGF signals for cell proliferation and migration through different pathways. Cytokine Growth Factor Rev. **11:**295–302.

11. **Boring, C. C., T. S. Squires, T. Tong, and S. Montgomery.** 1994. Cancer statistics, 1994. CA Cancer J. Clin. **44:**7–26.
12. **Bouvet, M., J. Spernyak, M. H. Katz, R. V. Mazurchuk, S. Takimoto, R. Bernacki, Y. M. Rustum, A. R. Moossa, and R. M. Hoffman.** 2005. High correlation of whole-body red fluorescent protein imaging and magnetic resonance imaging on an orthotopic model of pancreatic cancer. Cancer Res. **65:**9829–9833.
13. **Brembeck, F. H., F. S. Schreiber, T. B. Deramaudt, L. Craig, B. Rhoades, G. Swain, P. Grippo, D. A. Stoffers, D. G. Silberg, and A. K. Rustgi.** 2003. The mutant K-ras oncogene causes pancreatic periductal lymphocytic infiltration and gastric mucous neck cell hyperplasia in transgenic mice. Cancer Res. **63:**2005–2009.
14. **Caldas, C., S. A. Hahn, L. T. da Costa, M. S. Redston, M. Schutte, A. B. Seymour, C. L. Weinstein, R. H. Hruban, C. J. Yeo, and S. E. Kern.** 1994. Frequent somatic mutations and homozygous deletions of the p16 (MTS1) gene in pancreatic adenocarcinoma. Nat. Genet. **8:**27–32.
15. **Carstens, R. P., J. V. Eaton, H. R. Krigman, P. J. Walther, and M. A. Garcia-Blanco.** 1997. Alternative splicing of fibroblast growth factor receptor 2 (FGF-R2) in human prostate cancer. Oncogene **15:**3059–3065.
16. **Cavallaro, U., J. Niedermeyer, M. Fuxa, and G. Christofori.** 2001. N-CAM modulates tumour-cell adhesion to matrix by inducing FGF-receptor signalling. Nat. Cell Biol. **3:**650–657.
17. **Debnath, J., S. K. Muthuswamy, and J. S. Brugge.** 2003. Morphogenesis and oncogenesis of MCF-10A mammary epithelial acini grown in three-dimensional basement membrane cultures. Methods **30:**256–268.
18. **De Wever, O., and M. Mareel.** 2003. Role of tissue stroma in cancer cell invasion. J. Pathol. **200:**429–447.
19. **Doherty, P., and F. S. Walsh.** 1996. CAM-FGF receptor interactions: a model for axonal growth. Mol. Cell. Neurosci. **8:**99–111.
20. **Esni, F., B. R. Johansson, G. L. Radice, and H. Semb.** 2001. Dorsal pancreas agenesis in N-cadherin-deficient mice. Dev. Biol. **238:**202–212.
21. **Gmyr, V., J. Kerr-Conte, B. Vandewalle, C. Proye, J. Lefebvre, and F. Pattou.** 2001. Human pancreatic ductal cells: large-scale isolation and expansion. Cell Transplant. **10:**109–121.
22. **Grille, S. J., A. Bellacosa, J. Upson, A. J. Klein-Szanto, F. van Roy, W. Lee-Kwon, M. Donowitz, P. N. Tsichlis, and L. Larue.** 2003. The protein kinase Akt induces epithelial mesenchymal transition and promotes enhanced motility and invasiveness of squamous cell carcinoma lines. Cancer Res. **63:**2172–2178.
23. **Grippo, P. J., P. S. Nowlin, M. J. Demeure, D. S. Longnecker, and E. P. Sandgren.** 2003. Preinvasive pancreatic neoplasia of ductal phenotype induced by acinar cell targeting of mutant Kras in transgenic mice. Cancer Res. **63:**2016–2019.
24. **Hagel, M., E. L. George, A. Kim, R. Tamimi, S. L. Opitz, C. E. Turner, A. Imamoto, and S. M. Thomas.** 2002. The adaptor protein paxillin is essential for normal development in the mouse and is a critical transducer of fibronectin signaling. Mol. Cell. Biol. **22:**901–915.
25. **Hazan, R. B., G. R. Phillips, R. F. Qiao, L. Norton, and S. A. Aaronson.** 2000. Exogenous expression of N-cadherin in breast cancer cells induces cell migration, invasion, and metastasis. J. Cell Biol. **148:**779–790.
26. **Hingorani, S. R., E. F. Petricoin, A. Maitra, V. Rajapakse, C. King, M. A. Jacobetz, S. Ross, T. P. Conrads, T. D. Veenstra, B. A. Hitt, Y. Kawaguchi, D. Johann, L. A. Liotta, H. C. Crawford, M. E. Putt, T. Jacks, C. V. Wright, R. H. Hruban, A. M. Lowy, and D. A. Tuveson.** 2003. Preinvasive and invasive ductal pancreatic cancer and its early detection in the mouse. Cancer Cell **4:**437–450.
27. **Hruban, R. H., R. E. Wilentz, and S. E. Kern.** 2000. Genetic progression in the pancreatic ducts. Am. J. Pathol. **156:**1821–1825.
28. **Ilic, D., Y. Furuta, S. Kanazawa, N. Takeda, K. Sobue, N. Nakatsuji, S. Nomura, J. Fujimoto, M. Okada, and T. Yamamoto.** 1995. Reduced cell motility and enhanced focal adhesion contact formation in cells from FAK-deficient mice. Nature **377:**539–544.
29. **Ishiwata, T., H. Friess, M. W. Buchler, M. E. Lopez, and M. Korc.** 1998. Characterization of keratinocyte growth factor and receptor expression in human pancreatic cancer. Am. J. Pathol. **153:**213–222.
30. **Islam, S., T. E. Carey, G. T. Wolf, M. J. Wheelock, and K. R. Johnson.** 1996. Expression of N-cadherin by human squamous carcinoma cells induces a scattered fibroblastic phenotype with disrupted cell-cell adhesion. J. Cell Biol. **135:**1643–1654.
31. **Jackson, D., J. Bresnick, I. Rosewell, T. Crafton, R. Poulsom, G. Stamp, and C. Dickson.** 1997. Fibroblast growth factor receptor signalling has a role in lobuloalveolar development of the mammary gland. J. Cell Sci. **110:**1261–1268.
32. **Kobrin, M. S., Y. Yamanaka, H. Friess, M. E. Lopez, and M. Korc.** 1993. Aberrant expression of type I fibroblast growth factor receptor in human pancreatic adenocarcinomas. Cancer Res. **53:**4741–4744.
33. **Leung, H. Y., W. J. Gullick, and N. R. Lemoine.** 1994. Expression and functional activity of fibroblast growth factors and their receptors in human pancreatic cancer. Int. J. Cancer **59:**667–675.
34. **Lewis, B. C., D. S. Klimstra, and H. E. Varmus.** 2003. The c-myc and PyMT oncogenes induce different tumor types in a somatic mouse model for pancreatic cancer. Genes Dev. **17:**3127–3138.
35. **Luo, Y., and G. L. Radice.** 2003. Cadherin-mediated adhesion is essential for myofibril continuity across the plasma membrane but not for assembly of the contractile apparatus. J. Cell Sci. **116:**1471–1479.
36. **Luo, Y., and G. L. Radice.** 2005. N-cadherin acts upstream of VE-cadherin in controlling vascular morphogenesis. J. Cell Biol. **169:**29–34.
37. **Morgenstern, J. P., and H. Land.** 1990. Advanced mammalian gene transfer: high titre retroviral vectors with multiple drug selection markers and a complementary helper-free packaging cell line. Nucleic Acids Res. **18:**3587–3596.
38. **Nieman, M. T., R. S. Prudoff, K. R. Johnson, and M. J. Wheelock.** 1999. N-cadherin promotes motility in human breast cancer cells regardless of their E-cadherin expression. J. Cell Biol. **147:**631–644.
39. **Noren, N. K., B. P. Liu, K. Burridge, and B. Kreft.** 2000. p120 catenin regulates the actin cytoskeleton via Rho family GTPases. J. Cell Biol. **150:**567–580.
40. **Perl, A. K., P. Wilgenbus, U. Dahl, H. Semb, and G. Christofori.** 1998. A causal role for E-cadherin in the transition from adenoma to carcinoma. Nature **392:**190–193.
41. **Scarpa, A., P. Capelli, K. Mukai, G. Zamboni, T. Oda, C. Iacono, and S. Hirohashi.** 1993. Pancreatic adenocarcinomas frequently show p53 gene mutations. Am. J. Pathol. **142:**1534–1543.
42. **Schaller, M. D.** 2004. FAK and paxillin: regulators of N-cadherin adhesion and inhibitors of cell migration? J. Cell Biol. **166:**157–159.
43. **Schlaepfer, D. D., and S. K. Mitra.** 2004. Multiple connections link FAK to cell motility and invasion. Curr. Opin. Genet. Dev. **14:**92–101.
44. **Schreiber, F. S., T. B. Deramaudt, T. B. Brunner, M. I. Boretti, K. J. Gooch, D. A. Stoffers, E. J. Bernhard, and A. K. Rustgi.** 2004. Successful growth and characterization of mouse pancreatic ductal cells: functional properties of the Ki-RAS oncogene. Gastroenterology **127:**250–260.
45. **Schutte, M., R. H. Hruban, J. Geradts, R. Maynard, W. Hilgers, S. K. Rabindran, C. A. Moskaluk, S. A. Hahn, I. Schwarte-Waldhoff, W. Schmiegel, S. B. Baylin, S. E. Kern, and J. G. Herman.** 1997. Abrogation of the Rb/p16 tumor-suppressive pathway in virtually all pancreatic carcinomas. Cancer Res. **57:**3126–3130.
46. **Smit, V. T., A. J. Boot, A. M. Smits, G. J. Fleuren, C. J. Cornelisse, and J. L. Bos.** 1988. KRAS codon 12 mutations occur very frequently in pancreatic adenocarcinomas. Nucleic Acids Res. **16:**7773–7782.
47. **Suyama, K., I. Shapiro, M. Guttman, and R. B. Hazan.** 2002. A signaling pathway leading to metastasis is controlled by N-cadherin and the FGF receptor. Cancer Cell **2:**301–314.
48. **Takaoka, M., H. Harada, T. B. Deramaudt, K. Oyama, C. D. Andl, C. N. Johnstone, B. Rhoades, G. H. Enders, O. G. Opitz, and H. Nakagawa.** 2004. Ha-Ras(G12V) induces senescence in primary and immortalized human esophageal keratinocytes with p53 dysfunction. Oncogene **23:**6760–6768.
49. **Takeichi, M.** 1993. Cadherins in cancer: implications for invasion and metastasis. Curr. Opin. Cell Biol. **5:**806–811.
50. **Takeichi, M., K. Hatta, A. Nose, and A. Nagafuchi.** 1988. Identification of a gene family of cadherin cell adhesion molecules. Cell Differ. Dev. **25**(Suppl.)**:**91–94.
51. **Vleminckx, K., L. Vakaet, Jr., M. Mareel, W. Fiers, and F. van Roy.** 1991. Genetic manipulation of E-cadherin expression by epithelial tumor cells reveals an invasion suppressor role. Cell **66:**107–119.
52. **Volk, T., and B. Geiger.** 1984. A 135-kd membrane protein of intercellular adherens junctions. EMBO J. **3:**2249–2260.
53. **Wagner, M., F. R. Greten, C. K. Weber, S. Koschnick, T. Mattfeldt, W. Deppert, H. Kern, G. Adler, and R. M. Schmid.** 2001. A murine tumor progression model for pancreatic cancer recapitulating the genetic alterations of the human disease. Genes Dev. **15:**286–293.
54. **Wang, A. Z., G. K. Ojakian, and W. J. Nelson.** 1990. Steps in the morphogenesis of a polarized epithelium. I. Uncoupling the roles of cell-cell and cell-substratum contact in establishing plasma membrane polarity in multicellular epithelial (MDCK) cysts. J. Cell Sci. **95:**137–151.
55. **Warshaw, A. L., and C. Fernandez-del Castillo.** 1992. Pancreatic carcinoma. N. Engl. J. Med. **326:**455–465.
56. **Wilentz, R. E., C. A. Iacobuzio-Donahue, P. Argani, D. M. McCarthy, J. L. Parsons, C. J. Yeo, S. E. Kern, and R. H. Hruban.** 2000. Loss of expression of Dpc4 in pancreatic intraepithelial neoplasia: evidence that DPC4 inactivation occurs late in neoplastic progression. Cancer Res. **60:**2002–2006.
57. **Xu, X., W. E. Li, G. Y. Huang, R. Meyer, T. Chen, Y. Luo, M. P. Thomas, G. L. Radice, and C. W. Lo.** 2001. Modulation of mouse neural crest cell motility by N-cadherin and connexin 43 gap junctions. J. Cell Biol. **154:**217–230.
58. **Yano, H., Y. Mazaki, K. Kurokawa, S. K. Hanks, M. Matsuda, and H. Sabe.** 2004. Roles played by a subset of integrin signaling molecules in cadherin-based cell-cell adhesion. J. Cell Biol. **166:**283–295.
59. **Zahir, N., and V. M. Weaver.** 2004. Death in the third dimension: apoptosis regulation and tissue architecture. Curr. Opin. Genet. Dev. **14:**71–80.
60. **Zegers, M. M., L. E. O'Brien, W. Yu, A. Datta, and K. E. Mostov.** 2003. Epithelial polarity and tubulogenesis in vitro. Trends Cell Biol. **13:**169–176.